T cell factor 1-expressing memory-like CD8+ T cells sustain the immune response to chronic viral infections.

Daniel T. Utzschneider[1,7,8], Mélanie Charmoy[2,7], Vijaykumar Chennupati[2,7], Laurène Pousse[2,7], Daniela Pais Ferreira[2], Sandra Calderon-Copete[3], Maxime Danilo[2], Francesca Alfei[1,9], Maike Hofmann[4], Dominik Wieland[4,5,6], Sylvain Pradervand[3], Robert Thimme[4], Dietmar Zehn[1,7,9] and Werner Held[2,7]

[1] Division of Immunology and Allergy, Department of Medicine, Lausanne University Hospital (CHUV), 1011 Lausanne, Switzerland

[2] Ludwig Center for Cancer Research, Department of Fundamental Oncology, University of Lausanne, 1066 Epalinges, Switzerland

[3] Lausanne Genomic Technologies Facility (LGTF), University of Lausanne, 1015 Lausanne, Switzerland

[4] Universitätsklinikum Freiburg, Klinik für Innere Medizin II, Gastroenterologie, Hepatologie, Endokrinologie und Infektiologie

[5] Spemann Graduate School of Biology and Medicine (SGBM), University of Freiburg

[6] Faculty of Biology, University of Freiburg

[7] Equal contribution at first author level or at last author level.

Correspondence: Werner.Held@unil.ch

Present address:

[8] Department of Cellular and Molecular Medicine, UC San Diego, 9500 Gilman Dr., La Jolla, CA 92093-0377, USA

[9] Division of Animal Physiology and Immunology, School of Life Sciences Weihenstephan, Technical University of Munich, Freising, Germany

Running title: Tcf1 maintains the CD8 T-cell response in chronic infection

Keywords: Chronic infection, Differentiation of cytotoxic T-cells, T-cell exhaustion, T-cell memory, Tcf1, LCMV, PD-1

SUMMARY

Chronic infections promote the terminal differentiation (or exhaustion) of T-cells and are thought to preclude the formation of memory T-cells. Contrasting the latter, we discovered a small subpopulation of virus-specific CD8 T-cells that sustains the T-cell response in chronic infections. These cells are defined by - and depend on - the expression of the transcription factor Tcf1 (T cell factor 1) and show key characteristics of central memory cells while lacking an effector signature. Unlike conventional memory cells, Tcf1$^+$ T-cells display hallmarks of an “exhausted” phenotype, including the expression of certain inhibitory receptors, and these cells are critical for the cellular expansion in response to inhibitory receptor blockade. These findings identify a memory-like T-cell population as a prime target for therapeutic interventions to improve the immune response in chronic infections.

INTRODUCTION

The recognition of pathogen-derived antigens triggers a massive expansion of rare antigen-specific $CD8^+$ T-cells. Their progeny usually accumulate in large numbers of armed effector T-cells and these normally contribute to the eradication of viral pathogens (Williams and Bevan, 2007). In contrast, the immune system and specifically $CD8^+$ T-cells typically fail to eliminate the human immunodeficiency virus [HIV], the hepatitis C virus [HCV], or certain strains of the Lymphocytic choriomeningitis virus [LCMV] in mice. Nonetheless, such chronic infections go along with strong T-cell responses but compared to acutely resolved infections, T-cells in persisting infections typically show strong impairments in cytokine production (IFNγ, TNF and IL-2) and express high levels of inhibitory receptors such as PD-1 (programmed cell death-1) and Lymphocyte-activation gene 3 (Lag-3) (Klenerman and Hill, 2005; Kuchroo et al., 2014; Speiser et al., 2014; Virgin et al., 2009; Wherry, 2011; Wherry et al., 2007). These phenotypic changes along with the failure of the immune system to clear the pathogens lead to the concept that persisting infection exhaust a functional T-cell response, promote primarily terminally differentiated T-cells, and preclude the formation of $CD8^+$ T-cell memory (Mueller and Ahmed, 2009; Shin et al., 2007; Wherry et al., 2004; Williams and Bevan, 2007). Notwithstanding, these terminally differentiated effector cells persist in large numbers for extended periods of time and they still mediate a certain level of virus control. The latter is supported by the frequent emergence of T-cell epitope-escape variants in HIV infections (Price et al., 2004; Walker and McMichael, 2012) and observations that the depletion of $CD8^+$ T-cells from Rhesus macaques chronically infected with SIV severely increases virus titers (Jin et al., 1999; Schmitz et al., 1999). Moreover, anti-viral activity and the $CD8^+$ T cell response significantly improve when the signaling via inhibitory receptors such as PD-1 is prevented (Barber et al., 2006). All these observations indicate that the immune response has not irreversibly ceased. However, the molecular mechanisms that maintain the terminally differentiated T cells in chronic infections and that improve the T-cell response following check-point inhibition remain poorly understood.

While classical memory was so far not thought to form in chronic infections (Mueller and Ahmed, 2009; Shin et al., 2007; Wherry et al., 2004; Williams and Bevan, 2007), antigen-specific T-cell

populations were recently shown to undergo significant expansion following transfer into naïve host mice (Utzschneider et al., 2013). Based on all the aforementioned evidence we hypothesized that the prolonged presence of pathogen-specific $CD8^+$ T-cells in chronic viral infections depends on their generation from T-cells with strong expansion capacity and possible memory features (Speiser et al., 2014). The transcription factor Tcf1 (T-cell factor-1, encoded by the *Tcf7* gene) has a critical role in maintaining protective immunity after resolution of acute infections (Jeannet et al., 2010; Zhou et al., 2010). We thus postulated that a putative memory function in chronic infections might depend on Tcf1.

With the help of a newly generated Tcf1 reporter mouse strain and Tcf1 knockout mice we identify an antigen-specific $CD8^+$ T cell subpopulation, which is essential for sustaining the T-cell response in chronic infections and for the re-expansion of antigen-specific T-cells following inhibitory receptor blockade. This subpopulation displays a unique differentiation state. While it lacks an effector cell signature it displays multiple characteristics of central memory T-cells including regeneration capacity and the ability to produce differentiated effector T-cells. In contrast to conventional memory cells, $Tcf1^+$ CD8 T-cells also display the hallmarks of an “exhausted” phenotype including the expression of certain inhibitory receptors. Inhibitory receptor blockade expands this memory-like T cell population. Thus, we demonstrate a central role of memory-like cells for maintaining T-cell responses in chronic infections and for therapeutic interventions.

RESULTS

Normal expansion but impaired CD8 T-cell maintenance and virus control in the absence of Tcf1

The continuous presence of differentiated cells within a tissue can be explained by cellular longevity (Spalding et al., 2005), the replication and self-renewal of differentiated cells (Dor et al., 2004) or their de novo generation from a pool of undifferentiated precursor cells (Barker et al., 2007). We hypothesized that the prolonged presence of pathogen-specific $CD8^+$ T-cells in chronic viral infections depends on their generation from T-cells with memory function. The transcription factor Tcf1 (*Tcf7*) has a critical role in maintaining protective immunity after resolution of acute infections (Jeannet et al., 2010; Zhou et al., 2010). We therefore postulated that a putative memory function in chronic infections depends on Tcf1. To test this, $Tcf7^{-/-}$ [KO] or wild type [Wt] mice were inoculated with the LCMV clone-13 [c13] strain, which establishes a chronic infection. The two strains had similar frequencies of $CD8^+$ T-cells specific for the LCMV-derived gp33 and gp276 epitopes on day 8 (d8) post-infection (**Figure 1A**) but 8 weeks later KO mice had reduced frequencies of epitope-specific T-cells (**Figure 1B**). In agreement with these observations, both mouse strains showed initially similar virus titers in the kidneys and the blood (**Figure 1C, E**), but KO mice failed to control LCMV c13 infection (**Figure 1D, E**). Thus, Tcf1 expression is dispensable for the initial T-cell expansion but essential for the long-term maintenance of the T-cell response and pathogen control.

To determine whether the defect in maintaining KO T-cells was $CD8^+$ T-cell intrinsic, we transferred small numbers of Wt or KO $CD8^+$ T-cells expressing a gp33-specific transgenic TCR [P14 T-cells] into CD45 congenic C57BL/6 [B6] hosts. While Wt and KO P14 T-cells had accumulated in similar numbers 8 days after LCMV c13 infection (**Figure 1F**), tenfold fewer KO than Wt P14 T-cells were detected at d28 (**Figure 1G**). A similar difference was observed using Vβ5 transgenic host mice (**Figure 1H, S1C**), which show a reduced endogenous T-cell response to LCMV and, similar to CD4-depleted B6 mice, higher c13 titers than B6 (Utzschneider et al.,

2013). Of note, virus titers were comparably high in Vβ5 hosts with Wt or KO P14 cells (data not shown), indicating that Wt and KO P14 cells are in similar infectious and inflammatory environments. The reduced persistence of KO P14 cells was also not due to their elimination by the host. Indeed, chronically infected Vβ5 hosts with residual KO P14 cells did not reject freshly transferred KO P14 cells (**Figure S1)**. Altogether, we conclude that the absence of Tcf1 impairs the long-term maintenance of the CD8 T-cell response in chronic infections in a cell intrinsic fashion.

T-cell differentiation remains unaltered in the absence of Tcf1

As the long-term maintenance of KO P14 T-cells was reduced we next addressed whether this was associated with altered T-cell differentiation. On d8 post infection, KO and Wt P14 T-cells displayed similarly reduced abilities to co-produce TNF and IFNγ and comparably increased expression of PD-1 and Lag-3 (**Figure S2**). At the chronic phase of c13 infection (d28), the phenotypic and functional analysis of KO P14 T-cells was hampered by their low abundance. This prompted us to use Vβ5 recipient mice, which tolerate ten-fold higher P14 cell input without lethal immunopathology or virus elimination. These recipients harbor more P14 cells during chronic infection yet the difference between Wt and KO P14 cells is maintained **(Figure 1H**). Four weeks post infection, KO and Wt P14 T-cells displayed comparably high expression of PD-1, Lag-3 and GzmB (**Figure 2A-C**), and a similarly reduced ability to co-produce TNF and IFNγ (**Figure 2D**). The only difference was a minor reduction in the fraction of KO P14 T-cells producing IFNγ (**Figure 2E**). Thus, the initial expansion, effector differentiation and exhaustion remain unaltered while T-cell maintenance is severely compromised without Tcf1.

Tcf1 expression preserves the proliferative potential of T cells in chronic infection

We next investigated whether the impaired maintenance of KO T-cells stemmed from a decreased proliferative capacity. We tested this by transferring Wt and KO P14 cells obtained from chronic c13 infection into secondary recipients followed by LCMV Armstrong [Arm]

inoculation, which causes an acute infection (**Figure 3A**). Wt P14 T-cells underwent robust expansion in this setup (**Figure 3B)**, consistent with a prior report (Utzschneider et al., 2013). In contrast, KO P14 T-cells essentially failed to re-expand (**Figure 3B**).

Since re-expansion potential of chronically stimulated $CD8^+$ T cells depends on Tcf1, we next characterized Tcf1 expression by virus-specific Wt P14 T-cells in LCMV c13 infections. Tcf1 is expressed by all naive T-cells, a minor fraction of effector cells but by most memory T-cells found after a resolved acute LCMV infection (Boudousquie et al., 2014) (**Figure 3C**). In contrast, Tcf1 was expressed by a stable fraction of around 10% of Wt P14 T-cells throughout c13 infection in B6 recipients (**Figure 3C)** and in Vβ5 hosts **(Figure S3)** where viral titers are significantly higher. Together with the absence of re-expansion capacity of KO P14 cells, this strongly suggested that the proliferative capacity of wild type T-cells was confined to this $Tcf1^+$ subpopulation.

Tcf1 expressing T-cells maintain the immune response to chronic infection

To confirm the above observations in polyclonal T cells and to formally address whether the expansion capacity of Wt T-cells from chronic infections resides in the $Tcf1^+$ sub-population, we generated a Tcf1 reporter mouse strain. A bacterial artificial chromosome (BAC) containing the *Tcf7* locus was modified by the insertion of GFP (green fluorescent protein) into the translation start site present in exon 1 of *Tcf7* (**Figure S4A**). The modified BAC was used to generate transgenic mice.

We first ensured that GFP expression in reporter mice corresponded to that of Tcf1 protein. In agreement with intracellular Tcf1 staining, most $CD8^+$ T-cells expressed high levels of GFP (not shown). While B cells were negative for Tcf1 and for GFP, P14 T-cells from naive reporter mice were all GFP^+, which corresponded to Tcf1 protein expression (**Figure 4A**). We next verified the regulation of the Tcf1 reporter during chronic infection, as schematically shown in **Figure 4B**. Similar to Tcf1 protein expression, only around 10% of P14 reporter cells were GFP^+ at d28 of chronic infection (**Figure 4C, left**). Flow sorted GFP^+ P14 reporter cells were intracellular $Tcf1^+$, while Tcf1 was not detectable in sorted GFP^- P14 cells (**Figure 4C, right**), validating the reporter to track Tcf1-expressing $CD8^+$ T-cells during chronic infection.

We first used the reporter to investigate Tcf1 expression by polyclonal CD8 T cells specific for distinct LCMV epitopes. Very similar to Wt P14 cells, Tcf1-GFP was expressed by sub-populations of 6-10% of polyclonal CD8 T-cells specific for distinct LCMV epitopes (gp276, gp33 and np396) at d29 of c13 infection (**Figure S4B).** Thus, although np396 and gp276 tetramer$^+$ cells differ in their degree of "exhaustion" (Wherry et al., 2003), they contain similar subpopulations of Tcf1$^+$ cells. Notwithstanding, the epitope specificity of the cells impacts the absolute number of Tcf1$^+$ tetramer$^+$ cells.

Next we investigated the proliferative potential of polyclonal Wt Tcf1$^+$ and Tcf1$^-$ CD8$^+$ T-cells. Total CD8$^+$ spleen cells from chronically infected B6 reporter mice were separated into Tcf1-GFP$^+$ and Tcf1-GFP$^-$ populations and transferred into Vβ5 hosts prior to LCMV Arm infection (**Figure S4C)**. Eight days later, we observed a massive expansion of transferred Tcf1$^+$ CD8 T-cells specific for gp276, gp33 and np396. In comparison, the transferred Tcf1$^-$ CD8 T-cells essentially failed to re-expand (**Figure S4D, E)**. This showed that the re-expansion capacity of polyclonal CD8 T cells is confined to the Tcf1$^+$ sub-population. To compare the re-expansion potential of Tcf1$^+$ and Tcf1$^-$ T-cells that have an identical TCR we used monoclonal P14 reporter mice as schematically shown in **Figure 4B**. Tcf1-GFP$^+$ P14 T-cells isolated from chronically infected Vβ5 animals underwent robust expansion in LCMV Arm-infected secondary Vβ5 recipients, while the Tcf1-GFP$^-$ P14 population essentially failed to re-expand at day 8 post infection **(Figure 4D)**. The increased re-expansion capacity of Tcf1$^+$ cells correlated with an improved control of viral infection. While only occasional Vβ5 recipients that received no cells or Tcf1-GFP$^-$ P14 cells, had controlled LCMV Arm infection at d8 (1 of 11 mice; (9%) and 1/13 (8%), respectively), transfer of Tcf1-GFP$^+$ P14 cells led to viral control in spleen or blood in a considerable fraction of Vβ5 recipients (5 /13 (38%)). A corresponding effect was observed using polyclonal CD8 T cells (**Figure S4F**), indicating that Tcf1$^+$ cells have enhanced protective potential.

Interestingly, following re-challenge with LCMV Arm, descendants of P14 Tcf1-GFP$^+$ cells were mostly (90%) GFP$^-$, but a subpopulation of cells (~10%) was again GFP$^+$ (**Figure 4E**). Based on cell numbers, even Tcf1-GFP$^+$ cells had robustly expanded as compared to input (**Figure 4F**). On

the other hand P14 cells derived from transferred Tcf1-GFP$^-$ cells remained GFP$^-$ (**Figure 4E**). Corresponding data were obtained for polyclonal CD8 T-cell populations specific for gp276 and gp33 (**Figure S4G, H** and not shown). Thus, re-challenge of Tcf1$^+$ cells not only leads to the production of considerable numbers of more differentiated progeny but leads also to the expansion and thus the re-generation of Tcf1$^+$ cells.

We further tested if Tcf1-expressing cells are sufficient to sustain the immune response to chronic infection (**Figure 4G**). Tcf1-GFP$^-$ P14 T-cells, isolated from chronically infected recipients remained essentially undetectable following transfer into c13 infection-time-matched recipients. In contrast, cells derived from the Tcf1-GFP$^+$ population gradually increased over time (**Figure 4H, I**), which is remarkable since 10 times fewer Tcf1-GFP$^+$ than Tcf1-GFP$^-$ cells had been transferred. Again, the cells derived from transferred Tcf1-GFP$^+$ P14 T-cells were mainly GFP$^-$ cells but GFP$^+$ cells were also present (data not shown). We conclude that the T-cell response to chronic infection has a hierarchical structure whereby T cells expressing Tcf1 are necessary and sufficient to sustain the response.

Tcf1$^+$ cells from chronic infections have characteristics of memory and exhausted but not of effector T-cells.

To molecularly characterize Tcf1$^+$ CD8 T-cells we performed RNAseq analysis of Tcf1-GFP$^+$ P14 cells (chronic Tcf1$^+$) and Tcf1-GFP$^-$ P14 cells (chronic Tcf1$^-$) at d28 of LCMV c13 infection. The gene expression analysis further included naive P14 cells (naive) as well as Tcf1-GFP$^+$ and Tcf1-GFP$^-$ P14 cells at d28 of acute resolved LCMV Arm infection (Tcf1$^+$ memory and Tcf1$^-$ memory).

Principal component analysis applied to normalized RNA-seq gene read counts revealed that naïve cells, memory cells, chronic Tcf1$^-$ and chronic Tcf1$^+$ cells are distinct, while Tcf1$^+$ and Tcf1$^-$ memory cells are more closely related (**Figure 5A**). We further compared these data with available microarray data from effector, exhausted and memory CD8 T-cells obtained from LCMV Arm or c13 infected mice (Doering et al., 2012). As expected, this revealed similarity of all memory populations and of exhausted cells with chronic Tcf1$^-$ cells. The latter similarity is explained by the fact that 90% of P14 cells in chronic infection are Tcf1$^-$. These data validate the

combined analysis of the two datasets. Finally the data showed that effector cells are considerably more related to chronic Tcf1$^-$ than to chronic Tcf1$^+$ cells (**Figure 5B**). In agreement with these analyses, >2000 genes were differentially expressed in pairwise comparisons with naïve cells (False discovery rate (FDR) 5%) (**Figure S5A**) and unique sets of genes defined chronic Tcf1$^-$ cells (n=502) and chronic Tcf1$^+$ CD8 T-cells (n=498) (FDR 5%, Fold Change (FC)>2) (**Figure S5B, Table S1)**. Collectively, these data suggest that Tcf1$^+$ cells from chronic infections display a unique transcriptional profile.

We directly compared the gene expression profiles of chronic Tcf1$^+$ and Tcf1$^-$ cells (**Table S2**), which reside in the same host. Genes down-regulated in chronic Tcf1$^+$ cells were highly associated with the GO and KEGG pathway term "cell cycle" ($p=6.23e^{-33}$ and $p=8.08e^{-11}$, respectively) (**Table S3)**. Consistent with these findings, the expression of selected cell-division-related genes (*Mki67, Ccnb1, Plk1*, *Aurkb*) was low in chronic Tcf1$^+$ relative to chronic Tcf1$^-$ cells (**Fig. S6A**), indicating that the Tcf1$^+$ population is relatively quiescent yet harbors the capacity to mediate population expansion upon re-challenge.

We next determined whether chronic Tcf1$^+$ CD8 T-cells display hallmarks of memory cells, effector cells and/or exhausted CD8 T-cells. Gene set enrichment tests did not provide evidence for a significant enrichment of a memory signature (Doering et al., 2012) (generated relative to naive cells) in chronic Tcf1$^+$ cells (**Figure S5C**), which may be due to the fact that many memory genes are expressed in naive cells. Indeed, multiple genes required for the formation of CD8 T cell memory were expressed at higher levels in chronic Tcf1$^+$ as compared to Tcf1$^-$ P14 cells (*IL7r, Sell* (encoding CD62L)*, Ccr7, Id3, Bcl6*) (**Figure S6B**), whereby certain genes were expressed at higher levels in chronic Tcf1$^+$ CD8 T-cells as compared to Tcf1$^+$ memory cells or naive cells (*Id3, Bcl6*). Specific memory features were verified at the level of protein expression and extended using functional analyses. We detected significant CD62L and IL7Rα (CD127) expression selectively by Tcf1$^+$ cells, both by P14 and polyclonal CD8 T-cells **(Figure 5C, S6C)**. The ability to receive IL-7 signals may explain in part the maintenance of Tcf1$^+$ cells (Kaech et al., 2003). Further, a subpopulation of Tcf1$^+$ P14 cells expressed IL-2 (**Figure 5D**). Moreover, Tcf1$^+$ cells expressed Eomes and low levels of T-bet (*Tbx21*)(**Figure 5E, S6B, S6D**), similar to conventional

memory cells (Joshi et al., 2007). The low levels of T-bet in the Tcf1$^+$ precursor population was unexpected given that T-bet^{low} cells in chronic infections are reportedly terminally differentiated (Paley et al., 2012). However, Tcf1 is expressed by a relatively small subset of T-bet^{low} cells indicating that heterogeneity of the T-bet^{low} population may explain the apparent discrepancy. We conclude that Tcf1$^+$ CD8$^+$ T-cells in chronic infection exhibit striking similarities with central memory CD8$^+$ T-cells.

Conversely, gene set enrichment tests revealed a significant overlap of an effector gene signature (Doering et al., 2012) with chronic Tcf1$^-$ versus chronic Tcf1$^+$ cells (**Figure 5F**), indicating that chronic Tcf1$^+$ cells lack effector cell features. Indeed, selected genes associated with effector CD8 T cell differentiation or function were expressed at low levels in chronic Tcf1$^+$ as compared to Tcf1$^-$ T-cells (*Klrg1, Cx3cr1, Gzma, Gzmb, Prf1, Tbx21, Id2, Prdm1*) (**Figure S6D**). Remarkably, the expression of these effector genes was even lower in chronic Tcf1$^+$ T-cells as compared to conventional memory cells, but not as low as in naive T-cells. Flow cytometry analysis confirmed the absence of GzmB and KLRG1 in Tcf1$^+$ but presence in chronic Tcf1$^-$ cells (**Figure 5G**, **S6E**). Thus, Tcf1$^+$ cells generally lack the hallmarks of effector CD8 T cells.

We next addressed whether Tcf1$^+$ T-cells displayed hallmarks of exhausted T-cells or whether this phenotype was acquired during the expansion and differentiation of Tcf1$^+$ to Tcf1$^-$ cells. Interestingly, an exhaustion gene signature (Doering et al., 2012) was not enriched in chronic Tcf1$^-$ cells relative to chronic Tcf1$^+$ (**Figure S5D**). As chronic Tcf1$^-$ cells are very similar to exhausted cells (see e.g. the PCA) we conclude that chronic Tcf1$^-$ and Tcf1$^+$ cells predominantly share an exhaustion gene signature. In agreement with these data, specific exhaustion associated genes were expressed comparably by chronic Tcf1$^+$ and Tcf1$^-$ cells (*Pdcd1, Lag3, c-Maf*) (**Figure S6F**), which was confirmed by flow cytometry for PD-1 and Lag-3 both in P14 and in polyclonal T cells (**Figure 5H, S6G**). Thus Tcf1$^+$ T-cells displayed multiple hallmarks of exhausted T-cells. Further, the gene set enrichment tests indicated that small fractions of exhaustion genes are preferentially expressed by either Tcf1$^+$ or Tcf1$^-$ cells (**Figure S5D**). Indeed, specific exhaustion genes were expressed at low levels in Tcf1$^+$ T-cells (*Cd244, Havcr2* (Tim3*), Ccl3*) while *Ctla4 was* expressed at higher levels Tcf1$^+$ as compared to Tcf1$^-$ T-cells (**Figure S6F)**.

Functionally, Tcf1$^+$ T-cells produced slightly more IFNγ than Tcf1$^-$ cells, but slightly fewer of the IFNγ^+ cells co-produced TNF (**Figure 5I**). This feature may reflect the relative absence of effector differentiation of Tcf1$^+$ cells, rather than exhaustion. Thus, Tcf1$^+$ CD8$^+$ T-cells in chronic infections show a unique differentiation state, with a relative absence of effector differentiation but characteristics of memory CD8$^+$ T-cells together an exhausted phenotype.

The presence of Tcf1$^+$ T cells in chronic infection requires Tcf1 expression

We next sought to address whether Tcf1 expression was of relevance for the presence and/or the function of the Tcf1$^+$ T cell population. To this end, we generated P14 Tcf1-GFP reporter mice that do not express Tcf1 protein (KO reporter). P14 KO reporter cells isolated from naive mice retained high GFP expression (**Figure 5K**), indicating that the activity of the *Tcf7* locus does not depend on the Tcf1 protein and that the KO reporter could be used to follow "Tcf1$^+$ T cells lacking Tcf1 protein". As expected, Wt P14 reporter cells responding to c13 infection contained a sizeable population of Tcf1-GFP$^+$ cells. In contrast, when using KO reporter cells, the fraction and the number of Tcf1-GFP$^+$ cells were strongly reduced at d8 and d28 of c13 infection (**Figure 5L**). To independently confirm the absence of Tcf1-GFP$^+$ cells, we exploited the gene expression analysis and identified Slamf6 (Ly108) as a specific marker of Wt Tcf1-GFP$^+$ P14 cells (**Figure 5M**). High-level Slamf6 (Ly108) expression defined >6% of total Wt P14 cells but only around 1% of KO P14 cells (**Figure 5M**). We conclude that Tcf1$^+$ Slamf6^{hi} CD8 T-cells in chronic infections depend on Tcf1 protein expression. The absence of these Tcf1$^+$ Slamf6^{hi} CD8 T-cells in KO mice may account for the impaired maintenance of the T cell response to chronic infections.

Tcf1$^+$ T cell subpopulations exists in chronic human infections

We next determined if a similar Tcf1$^+$ subpopulation is also detectable among virus-specific CD8$^+$ T-cells in patients with chronic HCV infection. We found that 20-60% of HCV-specific CD8$^+$ T-cells were Tcf1$^+$ (**Figure 6A-C**). This contrasts with the uniform Tcf1$^+$ phenotype of naive and central memory CD8$^+$ T-cells in healthy donors (**Figure 6B, C**). Very similar to the observations in LCMV c13 infection, Tcf1$^+$ HCV-specific cells display higher expression of the memory marker

CD127 than Tcf1$^-$ cells and they express PD-1 (**Figure 6D, E)**. These data provide evidence for the existence of Tcf1$^+$ CD8 T cells in human chronic infection.

The expansion of CD8 T cells in response to PD-1 blockade depends on Tcf1

Several studies have shown that blocking PD-1/PD-L1 interaction increases effector functions and proliferation of antigen specific CD8$^+$ T-cells and this coincides with a decrease in pathogen or malignant tumor load (Barber et al., 2006; Herbst et al., 2014; Sakuishi et al., 2010). While PD-1/PD-L1 blockade increases effector functions and proliferation of antigen specific CD8$^+$ T-cells, the exact mechanism underlying the enhanced immune response remains elusive. Based on theses findings, we tested if the expansion of CD8$^+$ T-cells upon blockade of the PD-1/PD-L1 interaction depends on Tcf1 (**Figure 7A**). In agreement with prior findings (Barber et al., 2006), PD-1/PD-L1 blockade in LCMV c13 infected mice increased the Wt P14 T-cell population compared to isotype control treated mice. In contrast, KO P14 T-cells failed to expand (**Figure 7B**). Thus the expansion of chronically stimulated CD8$^+$ T-cells in response to inhibitory receptor blockade depends on Tcf1 expression.

Importantly, PD-1/PD-L1 blockade resulted in an enlarged Wt Tcf1$^+$ P14 population (**Figure 7C)**. We thus addressed whether the expansion of antigen-specific T cells depended on the presence of Tcf1$^+$ cells. Indeed Tcf1-GFP$^+$ P14 T-cells from c13 infected primary recipients significantly expanded following transfer into infection time matched secondary recipients and treatmed with PD-1 mAb (**Figure 7D**). In contrast, PD-1 mAb had no significant effect on transferred Tcf1-GFP$^-$ P14 cells (**Figure 7E**). These data demonstrate that the effectiveness of this therapeutic intervention depends on the Tcf1$^+$ CD8 T-cell population.

DISCUSSION

The loss of certain T-cell functions together with the decline in T-cell numbers led originally to the hypothesis that persisting infections are concomitant with rapid deterioration of the T-cell response without the formation of memory T-cells. Here, we establish that long-term T-cell responses in chronic infections are maintained by a subpopulation of memory-like cells expressing Tcf1. While memory-like Tcf1$^+$ T cells lack a characteristic effector signature they share multiple molecular and functional properties with central memory cells. Both express Tcf1, IL7Rα, CD62L, *Ccr7, Id3* etc and have the potential to efficiently expand in response to antigen re-challenge, produce more differentiated progeny and regenerate themselves. These novel insights require a significant revision of the concept of T-cell differentiation in chronic infections. They highlight that the key principal guiding T-cell differentiation in response to acute infection, i.e. the generation of differentiated cells and less differentiated T-cells, which retain proliferative potential, is conserved in chronic infections. Thus, the findings provide a mechanistic explanation for how effector T-cell responses are maintained long-term and why such responses can select epitope-escape variants in late stage HIV infections (Price et al., 2004; Walker and McMichael, 2012) or control virus load in chronic SIV infections in Rhesus macaques (Jin et al., 1999; Schmitz et al., 1999). Along this line we show that Tcf1$^+$ cells have an enhanced potential to control virus infection as compared to Tcf1$^-$ cells. However, it is unlikely that Tcf1$^+$ cells contribute directly to viral control as they lack the hallmarks of effector CD8 T-cells. Rather, they contribute to viral control indirectly by sustaining the production of Tcf1$^-$ cells, which have limited potential to expand but have effector potential. Collectively, the functional properties Tcf1$^+$ cells suggest that these cells exert stem cell-like activity to maintain a productive T cell response to chronic infection.

Prior work has identified a sub-compartment of proliferating cells among chronically stimulated CD8$^+$ T cells, which expressed intermediate levels of PD-1 (PD-1^{int}), high levels of T-bet but not Eomes (Paley et al., 2012). These cells gave rise to non-proliferating PD-1^{hi} T-bet^{lo} Eomes$^+$ cells. The Tcf1$^+$ T-cells described herein express low levels of cell division related genes and are predominantly PD-1^{hi} T-bet^{lo} and Eomes$^+$. The difference to (Paley et al., 2012) is likely explained

by heterogeneity of the PD-1^{hi} T-bet^{low} population. Together, the findings suggest that the immune response to chronic infection comprises several distinct compartments whose precise hierarchical order remains to be investigated further. Irrespectively, our data show that Tcf1^{+} T-cells are sufficient to sustain the immune response to chronic infection, indicating that they have a privileged position in this hierarchy.

A key difference to central memory cells is that Tcf1^{+} T-cells display an exhausted phenotype, including the expression of co-inhibitory receptors such as PD-1 and Lag-3. Our data also demonstrate that the “exhausted” phenotype is predominantly established prior to terminal cell differentiation, at the stage of memory-like T-cells. Nevertheless, we also find inhibitory receptor genes, such as *2B4* or *Tim3,* which are expressed by Tcf1^{-} but not by Tcf1^{+} T-cells. Together, our data show that most of the chronic phenotype is present in memory-like cells but that certain parts are acquired during the transition into terminally differentiated Tcf1^{-} cells. The compartmentalization of inhibitory receptor expression predicts distinct cellular responses to inhibitory receptor blockade. For example Tim3 blockade will preferentially act on the terminally differentiated Tcf1^{-} cells. On the other hand PD-1 blockade will act on both Tcf1^{+} and on Tcf1^{-} cells. The former leads to the expansion of the population and production of Tcf1^{-} cells, as shown herein and discussed below, and the latter improves the effector capacity of Tcf1^{-} cells, consistent with in numerous prior studies (Speiser et al., 2014).

Blocking inhibitory signals mediated through PD-1/PD-L1 interaction improves immune responses to chronic infection and cancer. While it has been shown that this treatment significantly increases the number of pathogen-specific T cells, it remained so far unclear how these additional cells are generated. It was possible that the blockade somehow induces a certain level of proliferation in the entire pathogen-specific population. However, we show that PD-L1 or PD-1 blockade unleashes the expansion potential of Tcf1^{+} cells. These insights provide a proof of concept that Tcf1^{+} cells are susceptible to therapeutic interventions. Thus the therapeutic effects of PD-1/PD-L1 blockade possibly depend on the restoration of the effector capacity of differentiated T cells and the enhanced proliferation and differentiation of Tcf1^{+} cells. Interestingly, inhibitory receptor blockade increased the size of the Tcf1^{+} compartment itself. With

regard to the treatment of cancer patients, these findings raise the possibility that, in addition to the presence of a tumor antigen-specific immune response, the presence of Tcf-1$^+$ cells represents an additional condition for PD-1 blockade to produce significant therapeutic benefit.

In conclusion, we have identified a subpopulation of virus-specific CD8$^+$ T-cells during LCMV clone-13 infection that sustains the ongoing immune response and mediates memory-like function. These cells do not show evidence for effector differentiation, but show multiple similarities to central memory CD8$^+$ T-cells together with a so-called “exhausted” or chronic phenotype. We therefore propose to refer to these cells as memory-like T-cells associated with antigen persistence (T_{MAP}) to provide a specific term for this previously uncharacterized T-cell population. The existence of these cells suggests that memory specializes according to the particular conditions of T cell stimulation. All together, we are not only identifying a memory T-cell equivalent in chronic infection, but also providing proof-of-concept that T_{MAP} represent a target for therapeutic interventions against chronic infections and possibly malignant tumors.

EXPERIMENTAL PROCEDURES

Mice

Mouse strains, which are described in detail in supplemental methods, were bred and maintained in the SPF facility and infected in the conventional animal facility of the University of Lausanne. Experiments were performed in six-week-old or older mice in compliance with the University of Lausanne Institutional regulations and were approved by the veterinarian authorities of the Canton de Vaud.

Detailed descriptions of viral infection, in vivo antibody treatment, Purification of mouse T-cells and adoptive cell transfers, surface and intracellular staining, antibodies and flow cytometry as well as RNA seq analysis are provided in supplemental materials.

Data analyses

Bar graphs depict the mean ±sem or ±SD as indicated. Statistical analyses were performed using Prism 6.0 (Graphpad Software). Paired and non-paired *t* tests (two-tailed) were used according to the type of experiments. P-values ≤ 0.05 were considered significant (*: $p<0.05$; **: $p<0.01$; ***: $p<0.001$); *p*-values >0.05; non-significant (ns).

ACCESSION NUMBERS

The accession number for the RNA-seq data reported in this paper is GSE83978.

SUPPLEMENTAL INFORMATION

Supplemental Information includes six figures four tables, and Supplemental Experimental Procedures and can be found at

AUTHOR CONTRIBUTIONS

DTU, MC and CVK designed experiments, performed experimental work, analyzed the results of the murine studies and prepared figures. LP designed experiments, performed experimental work and analyzed results of the murine studies. DPF, MD and FA performed experimental work and analyzed results of the murine studies. RT designed experiments and analyzed results of the human samples. DT and DW designed experiments, performed experimental work and analyzed results of the human study. SC and SP analyzed the RNAseq data. DZ conceived the study, supervised the project and wrote the manuscript. WH conceived the study, supervised the project and wrote and revised the manuscript.

ACKNOWLEDGMENTS

We are grateful to L. Carrie and C. Fumey for mouse management, the UNIL Flow Cytometry Facility for assistance, the UNIL Genomic Technology Facility for RNAseq, D. Moradpour (CHUV) for providing initial HCV samples and M. Prlic (Fred Hutchinson) and A. Wilson (University of Lausanne) for feedback and comments. This work was supported in part by grants from the Swiss National Science Foundation (SNSF) (310030B_141178 and 310030_159598) to W.H. and “CRSII3_141879 and PP00P3_144883” to D.Z. and from the European research council (ERC) “337043-ProtecTC” to D.Z..

REFERENCES

Barber, D.L., Wherry, E.J., Masopust, D., Zhu, B., Allison, J.P., Sharpe, A.H., Freeman, G.J., and Ahmed, R. (2006). Restoring function in exhausted CD8 T cells during chronic viral infection. Nature *439*, 682-687.

Barker, N., van Es, J.H., Kuipers, J., Kujala, P., van den Born, M., Cozijnsen, M., Haegebarth, A., Korving, J., Begthel, H., Peters, P.J., and Clevers, H. (2007). Identification of stem cells in small intestine and colon by marker gene Lgr5. Nature *449*, 1003-1007.

Boudousquie, C., Danilo, M., Pousse, L., Jeevan-Raj, B., Angelov, G.S., Chennupati, V., Zehn, D., and Held, W. (2014). Differences in the transduction of canonical Wnt signals demarcate effector and memory CD8 T cells with distinct recall proliferation capacity. J Immunol *193*, 2784-2791.

Doering, T.A., Crawford, A., Angelosanto, J.M., Paley, M.A., Ziegler, C.G., and Wherry, E.J. (2012). Network analysis reveals centrally connected genes and pathways involved in CD8+ T cell exhaustion versus memory. Immunity *37*, 1130-1144.

Dor, Y., Brown, J., Martinez, O.I., and Melton, D.A. (2004). Adult pancreatic beta-cells are formed by self-duplication rather than stem-cell differentiation. Nature *429*, 41-46.

Herbst, R.S., Soria, J.C., Kowanetz, M., Fine, G.D., Hamid, O., Gordon, M.S., Sosman, J.A., McDermott, D.F., Powderly, J.D., Gettinger, S.N.*, et al.* (2014). Predictive correlates of response to the anti-PD-L1 antibody MPDL3280A in cancer patients. Nature *515*, 563-567.

Jeannet, G., Boudousquie, C., Gardiol, N., Kang, J., Huelsken, J., and Held, W. (2010). Essential role of the Wnt pathway effector Tcf-1 for the establishment of functional CD8 T cell memory. Proceedings of the National Academy of Sciences of the United States of America *107*, 9777-9782.

Jin, X., Bauer, D.E., Tuttleton, S.E., Lewin, S., Gettie, A., Blanchard, J., Irwin, C.E., Safrit, J.T., Mittler, J., Weinberger, L.*, et al.* (1999). Dramatic rise in plasma viremia after CD8(+) T cell depletion in simian immunodeficiency virus-infected macaques. J Exp Med *189*, 991-998.

Joshi, N.S., Cui, W., Chandele, A., Lee, H.K., Urso, D.R., Hagman, J., Gapin, L., and Kaech, S.M. (2007). Inflammation directs memory precursor and short-lived effector CD8(+) T cell fates via the graded expression of T-bet transcription factor. Immunity *27*, 281-295.

Kaech, S.M., Tan, J.T., Wherry, E.J., Konieczny, B.T., Surh, C.D., and Ahmed, R. (2003). Selective expression of the interleukin 7 receptor identifies effector CD8 T cells that give rise to long-lived memory cells. Nat Immunol *4*, 1191-1198.

Klenerman, P., and Hill, A. (2005). T cells and viral persistence: lessons from diverse infections. Nat Immunol *6*, 873-879.

Kuchroo, V.K., Anderson, A.C., and Petrovas, C. (2014). Coinhibitory receptors and CD8 T cell exhaustion in chronic infections. Curr Opin HIV AIDS *9*, 439-445.

Mueller, S.N., and Ahmed, R. (2009). High antigen levels are the cause of T cell exhaustion during chronic viral infection. Proceedings of the National Academy of Sciences of the United States of America *106*, 8623-8628.

Paley, M.A., Kroy, D.C., Odorizzi, P.M., Johnnidis, J.B., Dolfi, D.V., Barnett, B.E., Bikoff, E.K., Robertson, E.J., Lauer, G.M., Reiner, S.L., and Wherry, E.J. (2012). Progenitor and terminal subsets of CD8+ T cells cooperate to contain chronic viral infection. Science *338*, 1220-1225.

Price, D.A., West, S.M., Betts, M.R., Ruff, L.E., Brenchley, J.M., Ambrozak, D.R., Edghill-Smith, Y., Kuroda, M.J., Bogdan, D., Kunstman, K.*, et al.* (2004). T cell receptor recognition motifs govern immune escape patterns in acute SIV infection. Immunity *21*, 793-803.

Sakuishi, K., Apetoh, L., Sullivan, J.M., Blazar, B.R., Kuchroo, V.K., and Anderson, A.C. (2010). Targeting Tim-3 and PD-1 pathways to reverse T cell exhaustion and restore anti-tumor immunity. J Exp Med *207*, 2187-2194.

Schmitz, J.E., Kuroda, M.J., Santra, S., Sasseville, V.G., Simon, M.A., Lifton, M.A., Racz, P., Tenner-Racz, K., Dalesandro, M., Scallon, B.J.*, et al.* (1999). Control of viremia in simian immunodeficiency virus infection by CD8+ lymphocytes. Science *283*, 857-860.

Shin, H., Blackburn, S.D., Blattman, J.N., and Wherry, E.J. (2007). Viral antigen and extensive division maintain virus-specific CD8 T cells during chronic infection. J Exp Med *204*, 941-949.

Spalding, K.L., Bhardwaj, R.D., Buchholz, B.A., Druid, H., and Frisen, J. (2005). Retrospective birth dating of cells in humans. Cell *122*, 133-143.

Speiser, D.E., Utzschneider, D.T., Oberle, S.G., Munz, C., Romero, P., and Zehn, D. (2014). T cell differentiation in chronic infection and cancer: functional adaptation or exhaustion? Nat Rev Immunol *14*, 768-774.

Utzschneider, D.T., Legat, A., Fuertes Marraco, S.A., Carrie, L., Luescher, I., Speiser, D.E., and Zehn, D. (2013). T cells maintain an exhausted phenotype after antigen withdrawal and population reexpansion. Nat Immunol *14*, 603-610.

Virgin, H.W., Wherry, E.J., and Ahmed, R. (2009). Redefining chronic viral infection. Cell *138*, 30-50.

Walker, B., and McMichael, A. (2012). The T-cell response to HIV. Cold Spring Harb Perspect Med *2*.

Wherry, E.J. (2011). T cell exhaustion. Nat Immunol *12*, 492-499.

Wherry, E.J., Barber, D.L., Kaech, S.M., Blattman, J.N., and Ahmed, R. (2004). Antigen-independent memory CD8 T cells do not develop during chronic viral infection. Proceedings of the National Academy of Sciences of the United States of America *101*, 16004-16009.

Wherry, E.J., Blattman, J.N., Murali-Krishna, K., van der Most, R., and Ahmed, R. (2003). Viral persistence alters CD8 T-cell immunodominance and tissue distribution and results in distinct stages of functional impairment. Journal of virology *77*, 4911-4927.

Wherry, E.J., Ha, S.J., Kaech, S.M., Haining, W.N., Sarkar, S., Kalia, V., Subramaniam, S., Blattman, J.N., Barber, D.L., and Ahmed, R. (2007). Molecular signature of CD8+ T cell exhaustion during chronic viral infection. Immunity *27*, 670-684.

Williams, M.A., and Bevan, M.J. (2007). Effector and memory CTL differentiation. Annu Rev Immunol *25*, 171-192.

Zhou, X., Yu, S., Zhao, D.M., Harty, J.T., Badovinac, V.P., and Xue, H.H. (2010). Differentiation and persistence of memory CD8(+) T cells depend on T cell factor 1. Immunity *33*, 229-240.

Figure 1

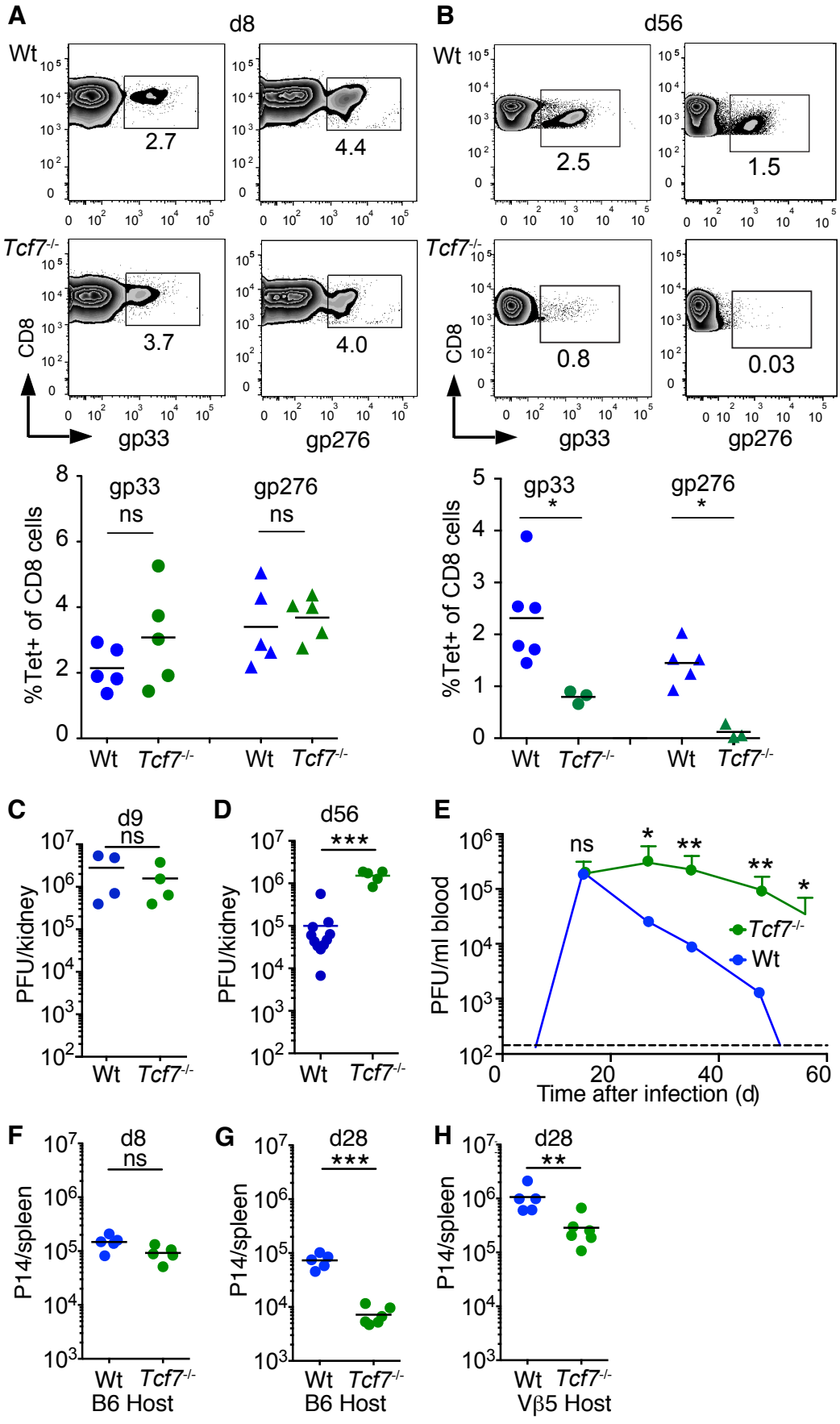
A
d8
Wt
2.7
4.4
Tcf7-/-
3.7
4.0
CD8
gp33
gp276
B
d56
Wt
2.5
1.5
Tcf7-/-
0.8
0.03
CD8
gp33
gp276
%Tet+ of CD8 cells
gp33
ns
gp276
ns
Wt
Tcf7-/-
Wt
Tcf7-/-
%Tet+ of CD8 cells
gp33
*
gp276
*
Wt
Tcf7-/-
Wt
Tcf7-/-
C
d9
ns
PFU/kidney
Wt
Tcf7-/-
D
d56
***
PFU/kidney
Wt
Tcf7-/-
E
PFU/ml blood
ns
*
**
**
*
Tcf7-/-
Wt
Time after infection (d)
F
d8
ns
P14/spleen
Wt
Tcf7-/-
B6 Host
G
d28
***
P14/spleen
Wt
Tcf7-/-
B6 Host
H
d28
**
P14/spleen
Wt
Tcf7-/-
Vβ5 Host

Figure 1: Normal expansion but impaired T-cell maintenance and virus control without Tcf1. C57/BL6 (Wt) or *Tcf7*$^{-/-}$ (KO) mice were infected with 2x10^6 PFU LCMV clone-13 (c13). The fraction of T-cells specific for gp33 and gp276 was determined on day 8 (**A**) or 56 (**B**) post infection using MHC tetramers. Representative CD8$^+$ gated flow cytometry plots and corresponding data graphs are shown. Virus titers were determined at day 9 (**C**) or day 56 (**D**) post infection in the kidney or at the indicated time points in the blood (**E**). (**F-H**) C57/BL6 mice (CD45.1$^+$ or CD45.1$^+$CD45.2$^+$) (**F, G**) or Vβ5 transgenic mice (CD45.1$^+$) (**H**) were engrafted with Wt or KO P14 T-cells (CD45.2$^+$) prior to infection with LCMV c13. P14 T-cell numbers were determined 8 (**F**) or 28 (**G**) days post-infection in the spleen of C57/BL6 mice and or on day 28 in Vβ5 transgenic mice (**H**). Each symbol (**A-D, F-H**) represents data from an individual mouse; small horizontal lines indicate the mean. Data are representative of two independent experiments with at least three mice per group (**A-D, F-H**) or combined from two independent experiments (**E**). Error bars=s.e.m.. ***p<0.001; **p<0.01; p<0.05. ns=not significant (p>0.05) based unpaired t-test. PFU: plaque-forming units. The broken line in **E** depicts the limit of detection.

Figure 2

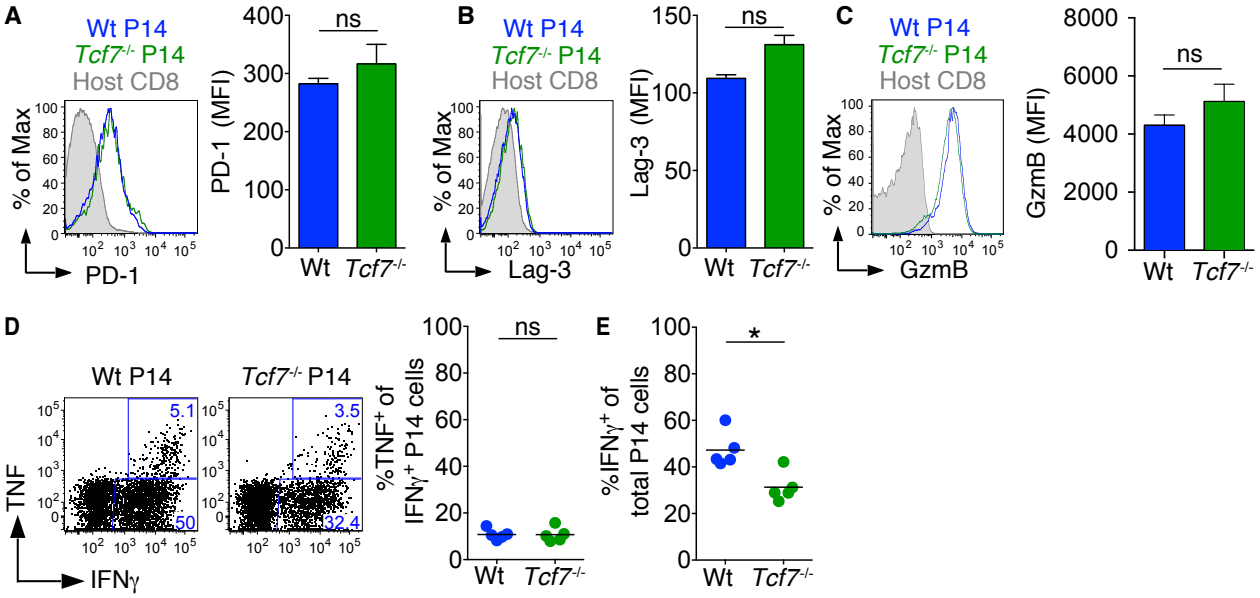

Figure 2: T-cell differentiation remains unchanged in the absence of Tcf1.

Vβ5 transgenic recipient mice were engrafted with either wild-type (Wt) or *Tcf7*$^{-/-}$ (KO) P14 T-cells and infected with LCMV c13. Splenocytes were analyzed 28 days post infection. PD-1 (**A**), Lag-3 (**B**) or Granzyme B (GzmB) (**C**) expression of KO (green) or wild-type (blue) P14 T-cells compared to host CD8^{+} T-cells (grey shadow, left) and calculated mean fluorescent intensity data (right). (**D, E**) Splenocytes were re-stimulated in vitro with gp33 peptide, intracellularly stained for IFNγ and TNF and analyzed by flow cytometry. Shown are representative flow cytometry plots of KO or wild-type P14 T-cells (**D, left**), the fraction of IFNγ^{+} P14 cells that co-produce TNF (**D, right**), and the frequency of P14 T-cells that produce IFNγ (**E**). Each symbol (**D, E**) represents data from an individual mouse; small horizontal lines indicate the mean. Data are representative of four independent experiments with at least five mice per group. Error bars (**A, B, C**), s.e.m. *p<0.05; ns=not significant (p>0.05) by unpaired t-test.

Figure 3

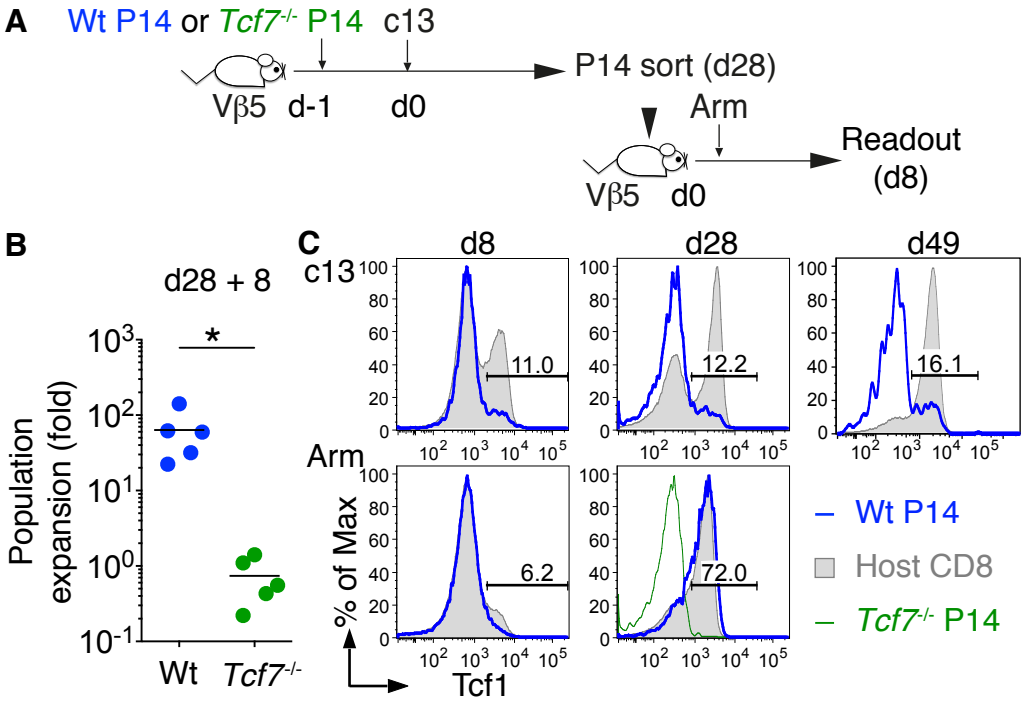

Figure 3: Tcf1 expression preserves proliferative potential of T cells in chronic infections.

(**A, B**) Vβ5 mice were engrafted with either *Tcf7*$^{-/-}$ (KO) or wild-type P14 T-cells and infected with LCMV c13. 4 weeks post-infection, P14 T-cells were re-isolated from spleen by flow cytometry-assisted cell sorting and transferred into naïve secondary Vβ5 host followed by an LCMV Armstrong (Arm) infection. (**B**) Population expansion of P14 T-cells in the secondary host 8 days after the LCMV Arm challenge relative to the engrafted cells. Engraftment was calculated assuming a 10% "take" of transferred cells. (**C**) C57/BL6 mice were engrafted with either KO or wild-type P14 T-cells prior to infection with LCMV c13 or Arm. Splenocytes were harvested at the indicated time points post infection and intracellularly stained for Tcf1. Shown are representative histograms of P14 T-cells (blue) compared to endogenous host CD8^{+} T-cells (grey shadow) or as a control with KO P14 T-cells (green). Numbers above the gates indicate the percentage of wild-type P14 T-cells expressing Tcf1. Each symbol (**B**) represents an individual mouse. Data are representative of two (**B**) or three (**C**) independent experiments, all with at least four mice per group and with similar results. *p<0.05 by unpaired t-test.

Figure 4

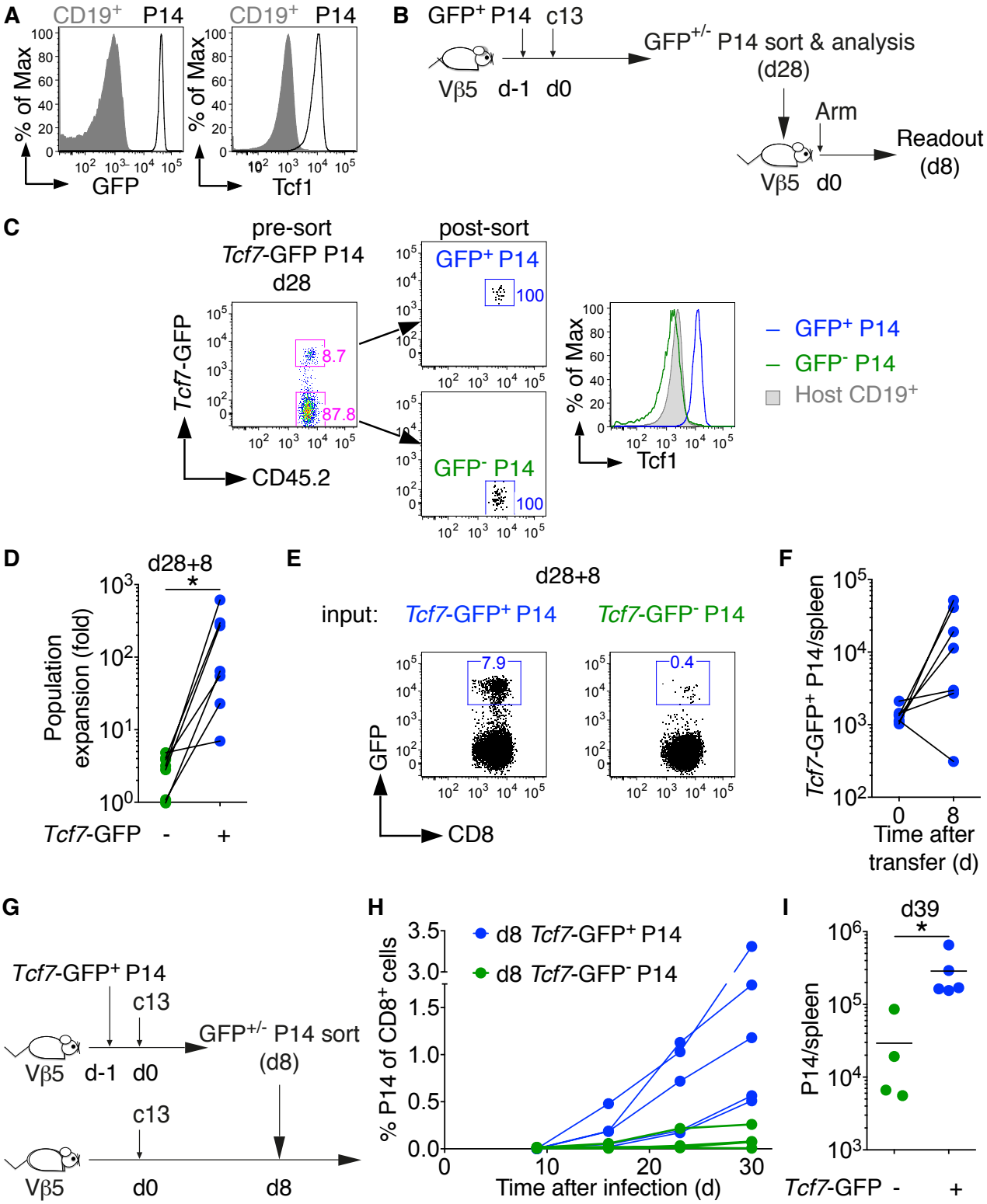

Figure 4: Only Tcf1 expressing T-cells retain robust proliferative potential in chronic infections.

(**A**) Validation of naïve Tcf1 P14 reporter mice. Shown is GFP (left) and Tcf1 (right) expression by $CD19^+$ B cells and P14 CD8 T-cells. (**B**) Experimental setup used in **C-F**. Vβ5 mice were engrafted with naïve Tcf1-GFP^+ P14 T-cells and infected with LCMV c13. Four weeks later, splenic P14 T-cells were separated into Tcf1-GFP^+ and Tcf1-GFP^- cells by flow cytometry-assisted cell sorting. Tcf1-GFP^+ and Tcf1-GFP^- P14 cells were separately transferred into secondary naïve Vβ5 mice, which were then challenged with LCMV Armstrong. (**C**) P14 T-cells before (left) and after (middle) the separation and confirmation that Tcf1-GFP^+ but not Tcf1-GFP^- P14 T-cells express Tcf1. (**D**) Population expansion (fold) of Tcf1-GFP^+ and Tcf1-GFP^- P14 T-cells in the secondary host 8 days after the LCMV Arm challenge. Shown are calculated population expansions assuming a 10% “take” of the transferred cells. Lines indicate Tcf1-GFP^+ and Tcf1-GFP^- derived from the same primary host. (**E**) Representative flow cytometry plots of GFP expression of re-expanded Tcf1-GFP^+ and Tcf1-GFP^- P14 T-cells and (**F**) absolute number of Tcf1-GFP^+ cells 8 days after the LCMV Arm challenge. (**G**) Experimental setup used in **H, I**. Vβ5 mice were engrafted with naïve Tcf1-GFP^+ P14 T-cells and infected with LCMV c13. Eight days post infection, splenic P14 T-cells were separated into Tcf1-GFP^+ and Tcf1-GFP^- cells by flow cytometry-assisted cell sorting and transferred into time-matched LCMV c13 infected Vβ5 mice. (**H**) Kinetics of appearance of P14 Tcf1-GFP^+ and Tcf1-GFP^- cells after the transfer. (**I**) Number of P14 cells per spleen (d30) derived from d8 transferred Tcf1-GFP+ (blue) or Tcf1-GFP- cells. Each symbol (**D, H**) represents data from an individual mouse. Data are representative of three (**A-E**) or two (**G-I**) independent experiments with at least three mice per group and with similar results. Statistical analysis ratio paired t-test.

Figure 5

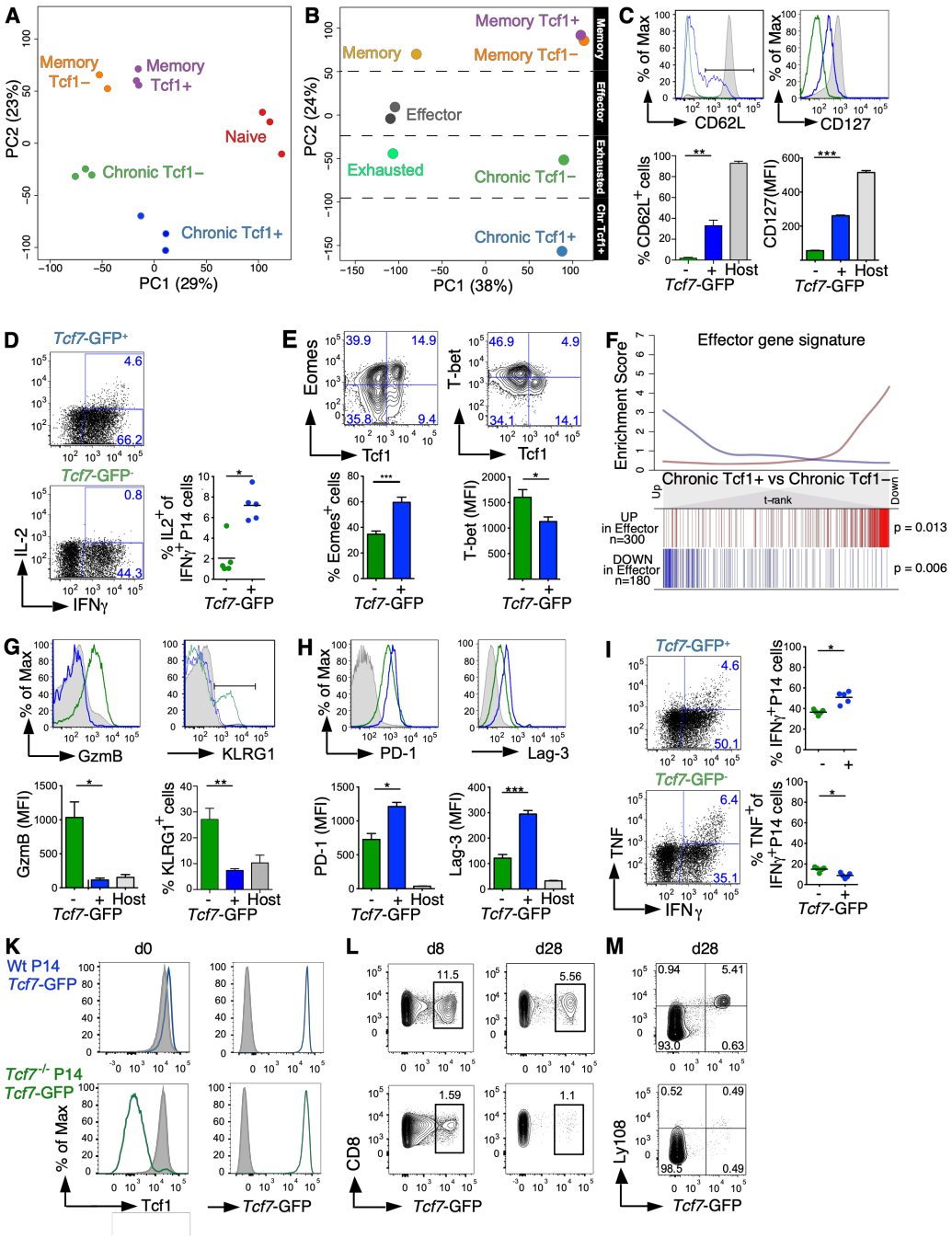

Figure 5: Molecular and phenotypic characterization of Tcf1$^+$ cells.

(**A-C**) Naive Tcf1-GFP$^+$ P14 T-cells (Naive) were transferred into Vβ5 or B6 mice, which were infected with LCMV c13 or Arm, respectively. Four weeks later Tcf1-GFP$^+$ and Tcf1-GFP$^-$ P14 cells were flow sorted and subjected to gene expression analysis using RNAseq.

(A) Principal component analysis (PCA) of normalized gene expression counts in naive P14 cells (Naive) (red), Tcf1+ and Tcf1- P14 cells obtained at d28 post LCMV Arm infection (Memory Tcf1$^+$,

(purple) and Memory Tcf1- (orange)) or at d28 post LCMV c13 infection (Chronic Tcf1$^-$ (green) and chronic Tcf1$^+$ (blue). Each dot represents an individual sample.

(**B**) PCA of genes differentially expressed between naive cells and the populations described above or between naive cells and populations obtained from virus-specific cells at d30 post LCMV Arm infection (Memory) (olive) (Memory), at d8 post LCMV Arm or c13 infection (Effector) (Black) and at d30 post for c13 infection (Exhausted) (light green) using published microarray data (Doering et al., 2012) (GSE41867). PCA was done on Z-scores from the comparisons versus naive. PC1 separates the two sets of experiments. PC2 separates the different cell types and groups memory populations together and exhausted cells with chronic Tcf1- cells. This validates the combination of the two data sets. Tcf1$^+$ cells from chronic infections are clearly distinct from all other populations.

(**C-I**) Vβ5 mice were engrafted with naïve Tcf1-GFP$^+$ or naïve Wt P14 T-cells and infected with LCMV c13. 4-5 weeks post-infection, splenocytes were surface and intracellularly stained for the indicated markers. Tcf1 positive or negative sub-fractions were distinguished by GFP expression or by intracellular Tcf1 staining. (**C**) Percentage of CD62L$^+$ cells and mean fluorescence intensity (MFI) of CD127 expression by Tcf1-GFP$^+$ (blue) or Tcf1-GFP$^-$ (green) P14 T-cells compared to Vβ5 host CD8$^+$ T-cells (grey shadow). (**D**) Splenocytes were re-stimulated *in vitro* with gp33-peptide and stained intracellularly for IFNγ and IL-2. Shown is the fraction of IFNγ^+ cells that produce IL-2 by gated Tcf1-GFP$^+$ or Tcf1-GFP$^-$ P14 T-cells. (**E**) Representative flow cytometry plots showing co-expression Tcf1 and Eomes (top left) or Tcf1 and T-bet in Wt P14 T-cells (top right). Corresponding bar graphs depict the percentage of Eomes$^+$ cells (bottom left) or the MFI of T-bet expression (bottom right) by Tcf1$^-$ (green) and Tcf1$^+$ P14 cells (blue).

(**F**) Gene set enrichment test of an effector gene signature (Doering et al. 2012) over the chronic Tcf1+ versus Chronic Tcf1- gene list ranked by the t-statistic. Barcode plots with relative enrichment scores for 300 up-regulated genes (red) and 180 down-regulated genes (blue) in the effector signature. There is a significant enrichment of the effector signature in chronic Tcf1$^-$ but not in chronic Tcf1$^+$ cells.

(**G**) MFI of Granzyme B (GzmB) expression (left) and percentage of KLRG1$^+$ cells and (**H**) MFI of PD-1 (left) or Lag-3 (right) by Tcf1-GFP$^+$ (blue) or Tcf1-GFP$^-$ (green) P14 T-cells compared to Vβ5 host CD8$^+$ T-cells (grey shadow).

(**I**) Splenocytes were re-stimulated *in vitro* with gp33-peptide and stained intracellularly for IFNγ and TNF. Shown are representative flow cytometry plots of Tcf1-GFP$^+$ or Tcf1-GFP$^-$ P14 T-cells (left), the fraction of Tcf1-GFP$^+$ or Tcf1-GFP$^-$ P14 T-cells that produce IFNγ (top right) or the fraction of IFNγ^+ Tcf1-GFP$^+$ or Tcf1-GFP$^-$ P14 T-cells that co-produce TNF (bottom right). Each symbol (**I**) represents an individual mouse; small horizontal lines indicate the mean. Data are representative of 2-4 independent experiments each with at least three mice per group. Error bars (**D, F- H**) s.e.m. Statistical analysis unpaired t-test.

(**K-M**) Analysis of Wt and KO P14 reporter T-cells. (**K**) Tcf1 and Tcf1-GFP expression by Wt (top) and KO P14 reporter T-cells (bottom) from naive mice. (**L**) Tcf1-GFP expression by Wt (top) and KO P14 reporter T-cells (bottom) at d8 (left) and d28 post LCMV c13 infection (right). (**M**) Ly108 (Slamf6) expression by Wt and KO P14 reporter T-cells at d28 post LCMV c13 infection. Data are representative of two independent experiments (one using Vβ5 and one using Wt recipients) both with 2-3 recipients per group and with similar results.

Figure 6

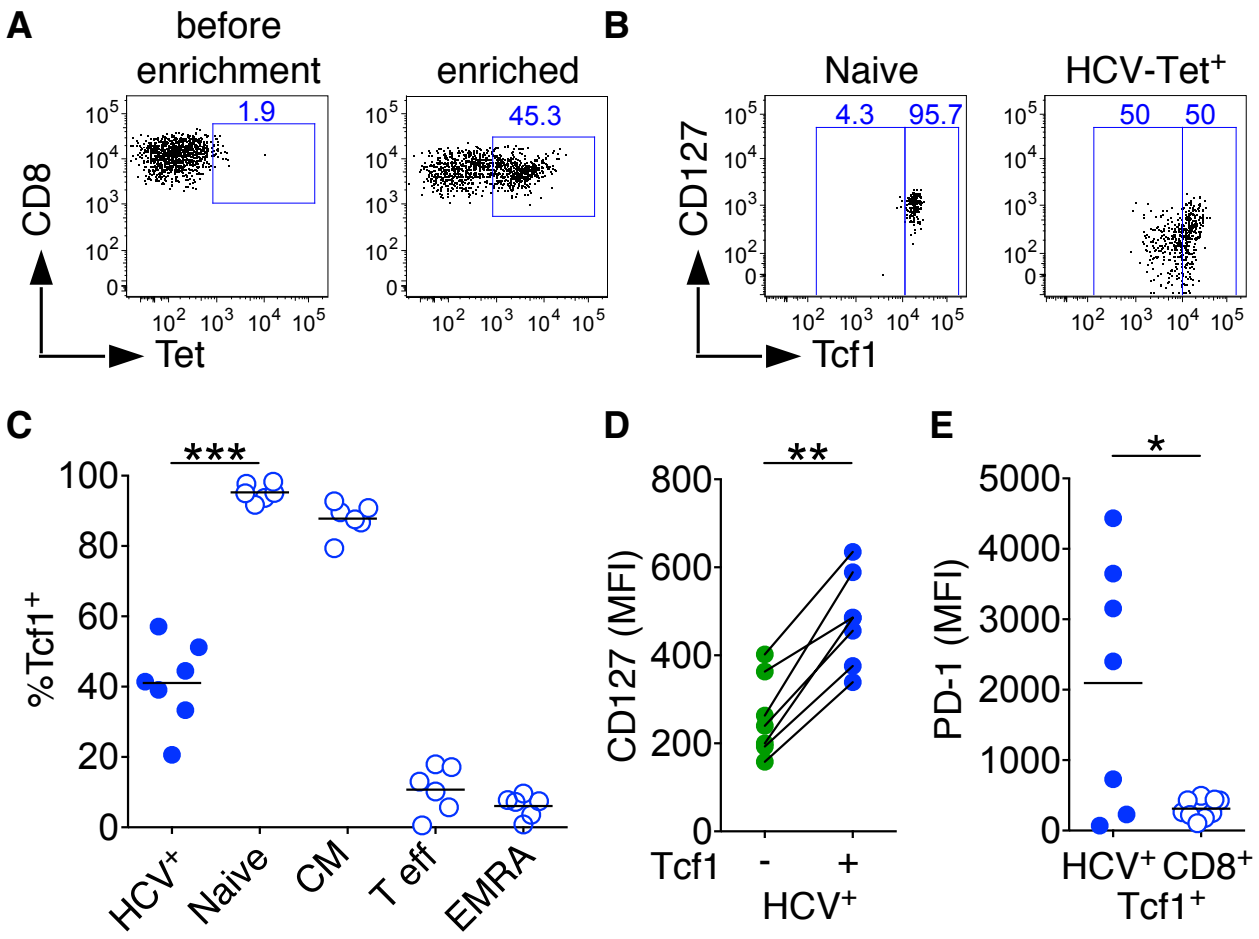

Figure 6: Tcf1$^+$ T-cells with memory characteristics in HCV infection.

HCV-specific CD8 T-cells were enriched from patients with chronic HCV infection (**A,** n=7) and analyzed for Tcf1 versus CD127 expression in comparison to naive CD8$^+$ T-cells from a healthy donor (**B,** n=6). **(c)** The fraction of Tcf1$^+$ HCV-specific T-cells was compared to the indicated CD8$^+$ T-cell subset in healthy donors. (**D)** MFI of CD127 expression in Tcf1$^+$ versus Tcf1$^-$ HCV-specific CD8$^+$ T-cells. (**E**) MFI of PD-1 expression in Tcf1$^+$ HCV-specific CD8$^+$ T-cells (filled dots) as compared to naïve CD8$^+$ T-cells from healthy donors (open dots). ***p<0.0001; **p<0.001; *p<0.05; ns=not significant (p>0.05) by paired or unpaired t-test.

Figure 7

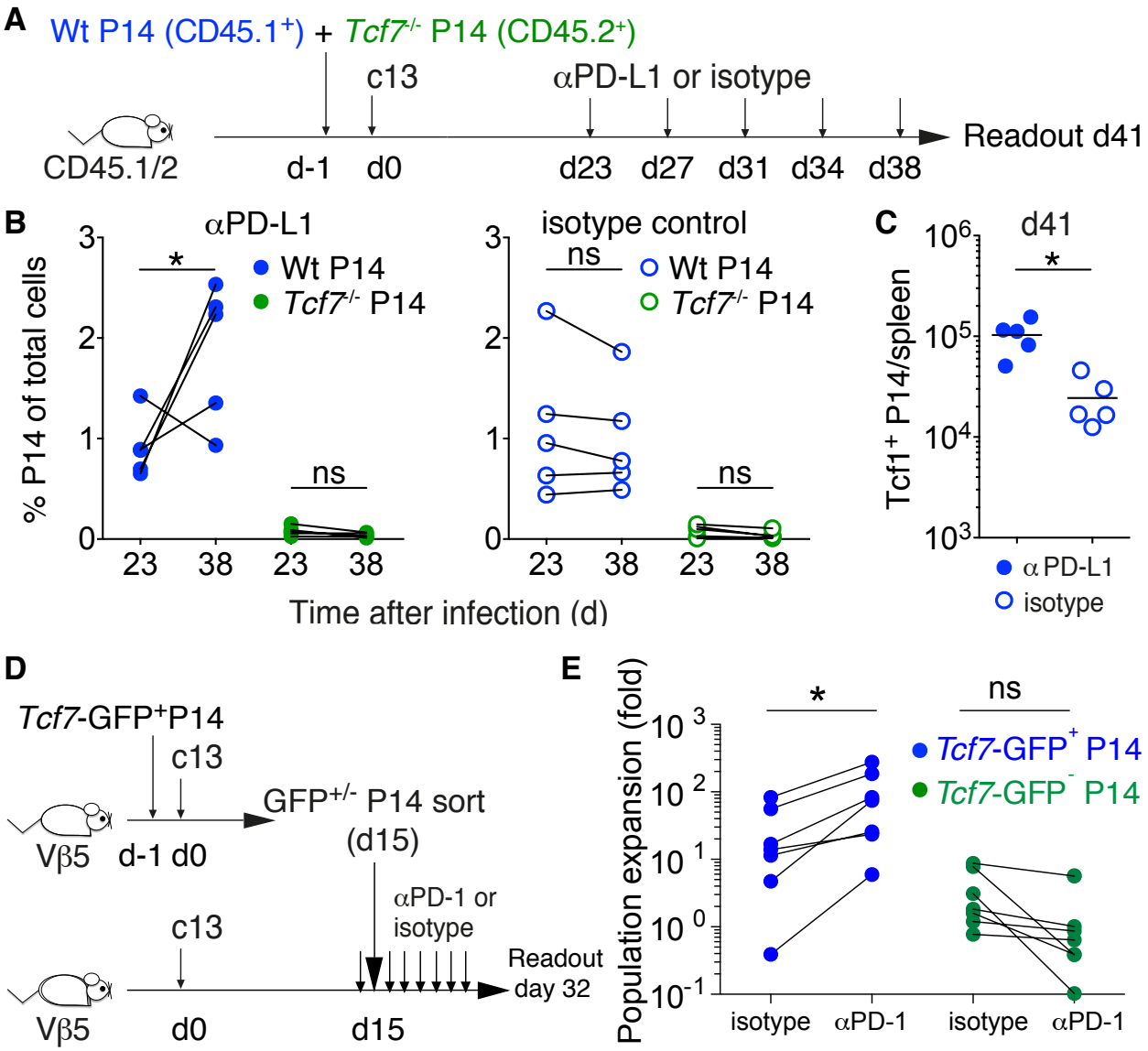

Figure 7: PD-1 induced re-activation of T-cells in chronic infections requires Tcf1⁺ T cells.

(**A**) Experimental setup used in **B, C**. CD45.2⁺ *Tcf7*$^{-/-}$ (KO) and CD45.1⁺ Wt P14 T-cells were co-transferred into CD45.1/2⁺ mice and subsequently infected with LCMV c13. Twenty-three days post-infection, mice were treated at 3-day intervals with 200 μg anti-PD-L1 antibody or an isotype control. (**B**) Frequency of KO and Wt P14 T-cells among total cells in the blood after administration of anti PD-L1 (left) or istoype control (right). (**C**) Absolute number of Tcf1⁺ Wt P14 T-cells after isotype or anti-PD-L1 treatment. Each symbol represents data from an individual mouse; small horizontal lines indicate the mean. Data are representative of two independent experiments (one anti-PD-L1 and one anti-PD-1), all with at least four mice per group and with

similar results. *p<0.05; ns=not significant (p>0.05) based on unpaired t-test. (**D**) Experimental setup used in **E**. Vβ5 mice were engrafted with naïve Tcf1-GFP$^+$ P14 T-cells and infected with LCMV c13. On d15 post infection, splenic P14 T-cells were flow sorted into Tcf1-GFP$^+$ and Tcf1-GFP$^-$ cells and transferred into c13 infection time-matched secondary Vβ5 mice. Secondary recipients were treated with anti-PD1 or isotype control antibody and analyzed on day 32-35. (**E**) Population expansion (fold) of Tcf1-GFP$^+$ and Tcf1-GFP$^-$ P14 T-cells in secondary recipients following treatment with anti-PD1 (αPD1) or isotype control Ab. Each symbol represents an individual secondary recipient, whereby recipients receiving input cells from one donor are connected with a line. Shown is the fold population expansion assuming a 10% “take” of transferred cells. Data are compiled from two independent experiments using a total of 8 or more mice per group. *p<0.05; ns=not significant (p>0.05) based on unpaired t-test.

Supplemental Figure 1

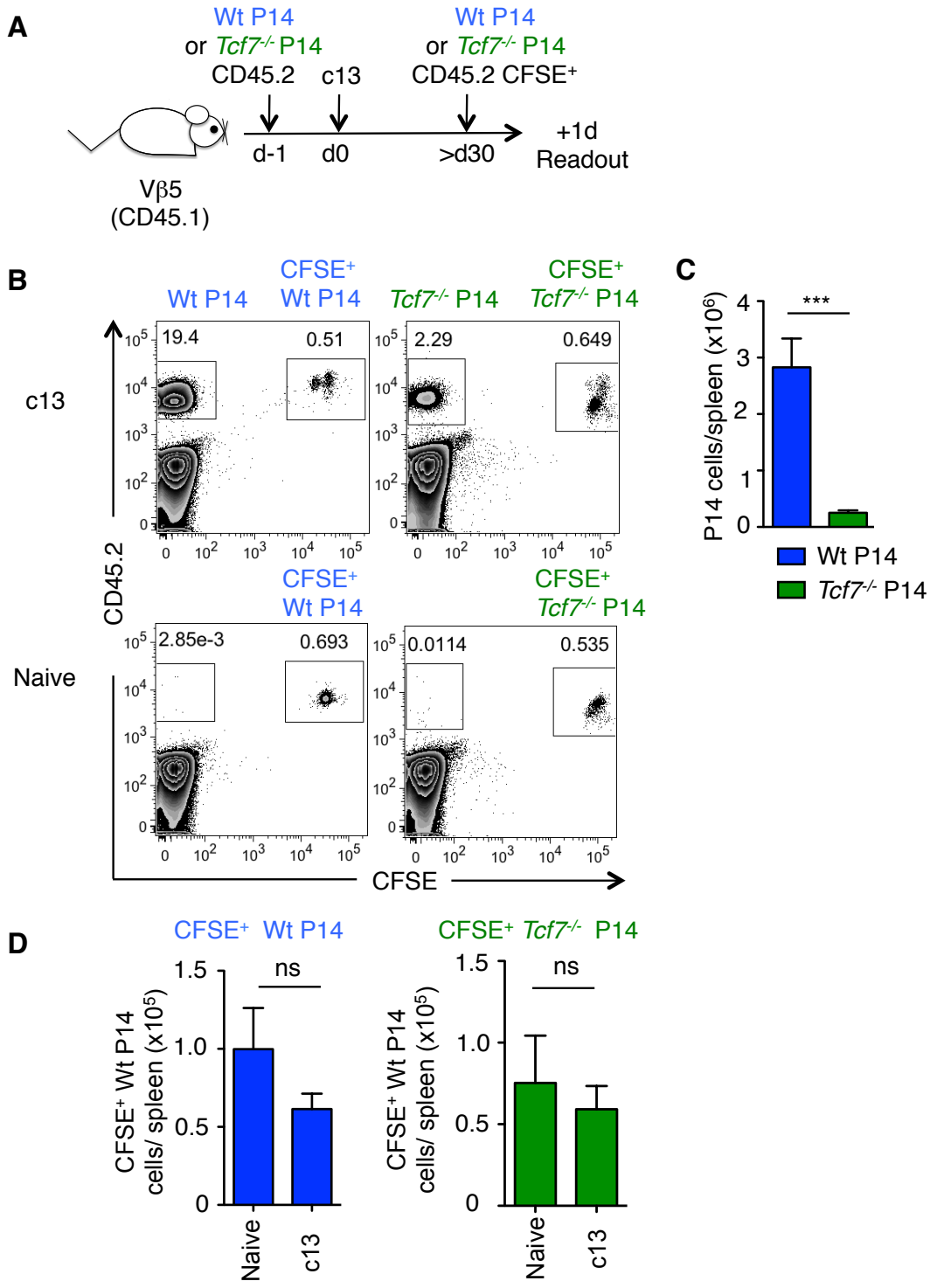

Figure S1, refers to Figure 1: The reduced abundance of *Tcf7*$^{-/-}$ P14 cells is not due to rejection by the host.
(**A**) Schematic representation of the experiment. Vβ5 mice (CD45.1^{+}) were engrafted with *Tcf7*$^{+/+}$ wild type (Wt) or *Tcf7*$^{-/-}$ P14 T cells (CD45.2^{+}) prior to infection with LCMV clone-13 (c13). Recipient mice received a secondary graft of CFSE-labeled (CFSE^{+}) naive Wt or *Tcf7*$^{-/-}$ P14 splenocytes (CD45.2^{+}), respectively, >d30 post c13 infection. In parallel, CFSE-labeled (CFSE^{+}) naive Wt or *Tcf7*$^{-/-}$ P14 splenocytes were injected into naive Vβ5 mice. The abundance of CFSE^{+} CD8^{+} CD45.2^{+} cells was determined one day later.

(**B**) Representative density plots show the presence of host cells ($CD45.2^-$ $CFSE^-$), the primary P14 graft ($CD45.2^+$ $CFSE^-$) and the secondary P14 graft ($CD45.2^+$ $CFSE^+$) among gated CD8 T cells in the spleen of c13 infected Vβ5 mice. Naive mice did not receive a primary graft and thus lack $CD45.2^+$ $CFSE^-$ cells. Numbers depict the percentage of cells in the respective gate.
(**C**) Number of Wt and *Tcf7*$^{-/-}$ P14 cells (primary graft) in recipient spleen, confirming a reduced abundance of *Tcf7*$^{-/-}$ P14 cells in c13 infected Vβ5 mice.
(**D**) Number of $CFSE^+$ Wt P14 cells (secondary graft) (left) and $CFSE^+$ *Tcf7*$^{-/-}$ P14 cells in the spleen of naive mice or c13 infected Vβ5 mice. There is no significant difference between naive and mice that previously received Wt or *Tcf7*$^{-/-}$ P14 cells, respectively. The bar graph shows mean ±SD (n=3) from a single experiment. ns; not significant, $p>0.05$ based on unpaired t-test.

Supplemental Figure 2

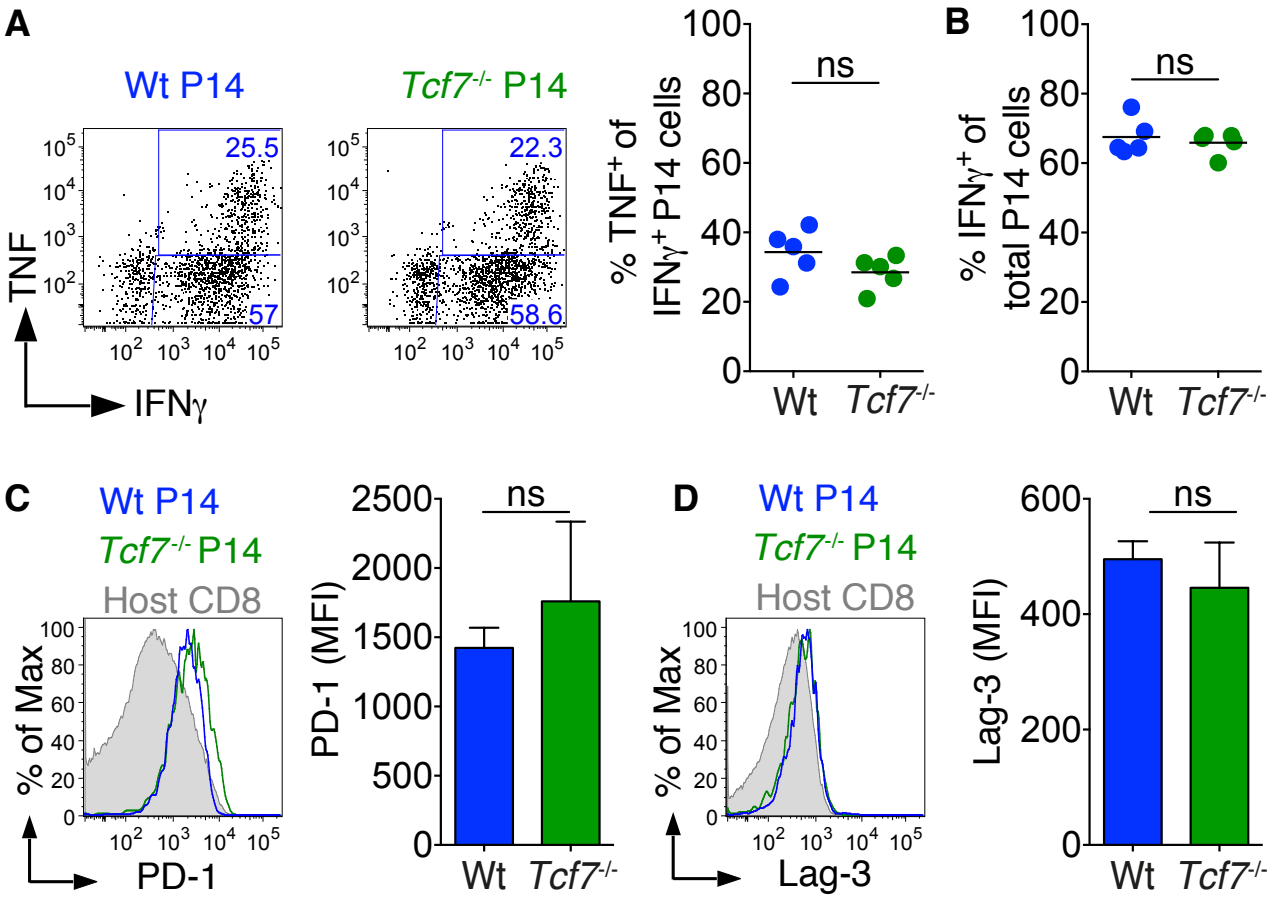

Figure S2, refers to Figure 2: Initial T cell differentiation remains unchanged in the absence of Tcf1.
C57/BL6 mice (CD45.1$^+$) were engrafted with *Tcf7*$^{-/-}$ or *Tcf7*$^{+/+}$ (wild type, Wt) P14 T cells (CD45.2$^+$) prior to infection with LCMV clone-13. (**A, B**) Splenocytes were re-stimulated with gp33-peptide *in vitro*, intracellularly stained for IFNγ and TNF and analyzed by flow cytometry. Shown are representative flow cytometry plots of Wt or *Tcf7*$^{-/-}$ P14 T cells (**A, left**), the fraction of IFNγ positive P14 cells that co-produce TNF (**A, right**), and the frequency of P14 T cells that produce IFNγ (**B**). (**C, D**) Representative PD-1 (**C**) and Lag-3 (**D**) expression histograms of d8 *Tcf7*$^{-/-}$ or Wt P14 T cells and total host CD8$^+$ T cells (left) and calculated mean fluorescent intensity (MFI) for all mice (right). Each symbol (**A, B**) represents an individual mouse; small horizontal lines indicate the mean. Data are representative of two independent experiments with at least five mice per group. Error bars (**C, D**), s.e.m. Statistical analysis unpaired t-test.

Supplemental Figure 3

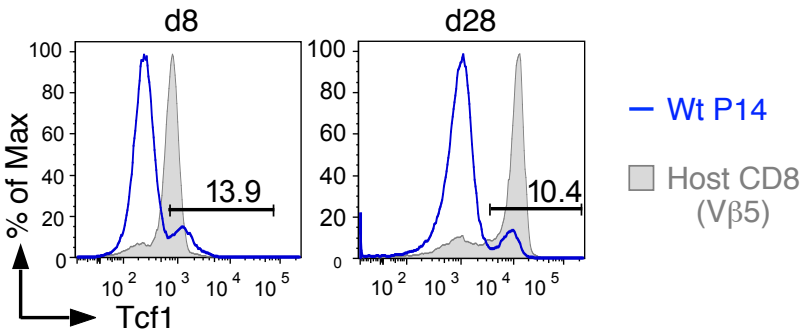

Figure S3, refers to Figure 3: Tcf1 expression in Wt P14 cells responding to c13 in Vβ5 recipients
Schematic representation of the experiment: Vβ5 mice were engrafted with Wt P14 T cells prior to infection with LCMV c13. Splenocytes were harvested and intracellularly stained for Tcf1 expression at d8 or d28 post infection. Representative histogram overlays showing Tcf1 expression by P14 T cells (blue) compared to endogenous host $CD8^+$ T cells (grey fill). Numbers depict the percentage of P14 T cells expressing Tcf1. Data are representative of two independent experiments, each with at least three mice per group and with similar results.

Supplemental Figure 4

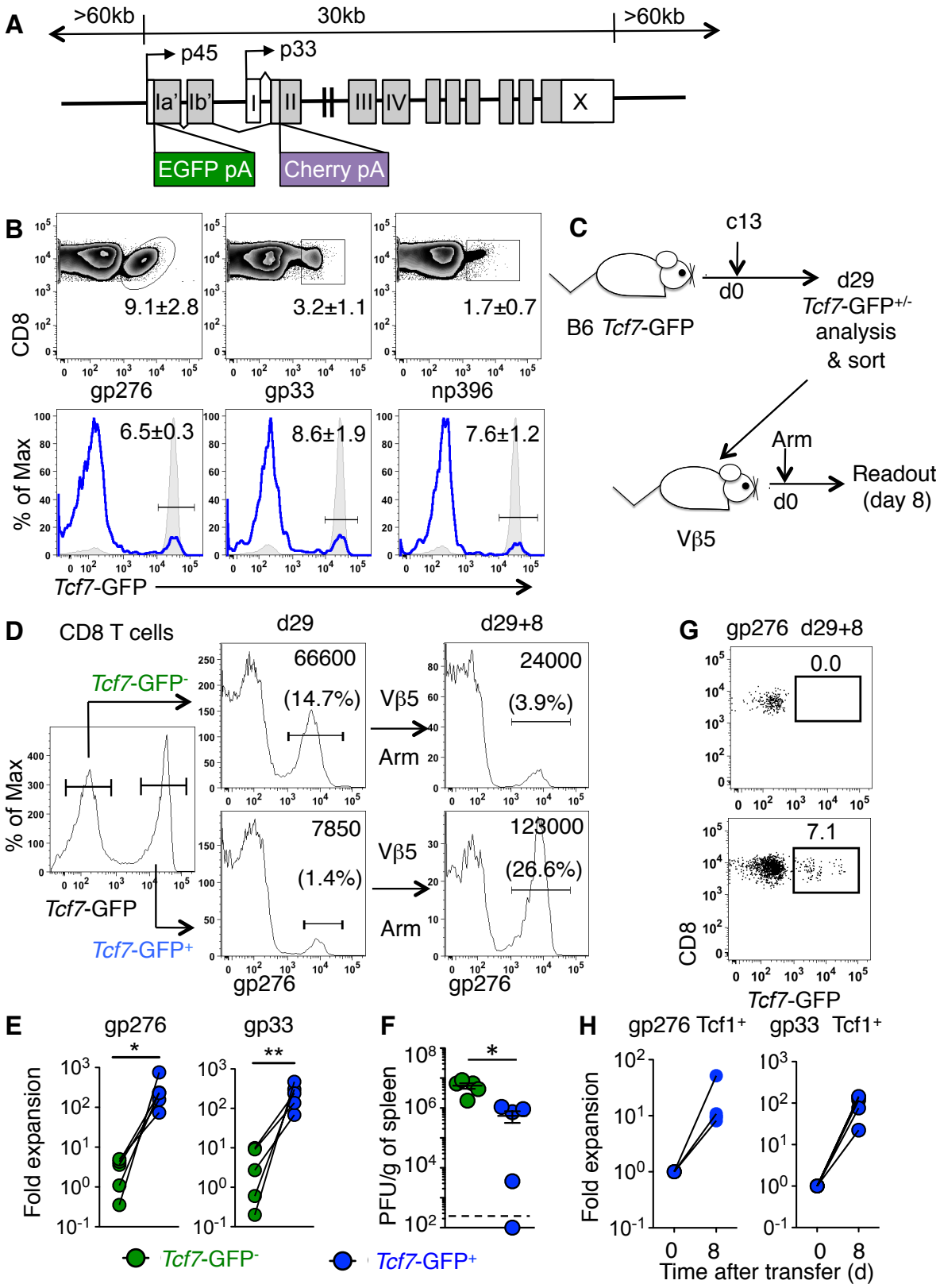

Figure S4, refers to Figure 4: Analyses of polyclonal CD8 T cells responding to c13 using Tcf1 reporter mice
(**A**) A bacterial artificial chromosome (BAC) containing the murine *Tcf7* locus was modified by inserting EGFP into the first translation codon of the Tcf1 open reading frame. In addition, mCherry, was inserted into a downstream

translation codon to prevent the expression of a dominant negative Tcf1 isoform. The modified BAC was used to generate transgenic mice on a B6 background.

(**B**) B6 *Tcf7*-GFP reporter mice were analyzed for gp276, gp33 and np396 tetramer staining among CD8 T cells at day 29 of LCMV c13 infection (top). Representative histograms show *Tcf7*-GFP expression in gated tetramer$^+$ cells (blue) as compared to CD44$^-$ (naive) CD8 T cells (grey fill). Numbers depict the mean percentage (±SD) of tetramer$^+$ cells among total CD8 T cells (top) or of *Tcf7*-GFP$^+$ cells among gated tetramer$^+$ cells of n=5 mice.

(**C**) Schematic outline of the experimental approach. B6 *Tcf7*-GFP reporter mice were infected with LCMV c13 and 29 days later *Tcf7*-GFP$^+$ and *Tcf7*-GFP$^-$ CD8 T cells were analyzed using tetramer or flow sorted and transferred into Vβ5 mice, which were then infected with LCMV Arm. Eight days later donor-derived CD8 T cells (CD45.2$^+$) were analyzed using tetramer.

(**D**) Representative histograms show GFP expression among CD8 T cells from the spleen of c13 infected B6 *Tcf7*-GFP reporter mice (left) and the analysis of gated *Tcf7*-GFP$^+$ and *Tcf7*-GFP$^-$ CD8 T cells with gp276 tetramers (middle). After transfer of *Tcf7*-GFP$^+$ or *Tcf7*-GFP$^-$ CD8 T cells into Vβ5 recipients and re-challenge with LCMV Arm, gated CD8 T cells present in the spleen were analyzed using tetramers (right). Numbers depict the fraction of gp276 tetramer$^+$ cells among total CD8$^+$ T cells present in the spleen.

(**E**) The number of gp276 or gp33 tetramer$^+$ cells in the input (d29) and the output splenocyte population (d29+8) was used to calculate the fold expansion of tetramer+ cells, assuming 10% take of the transferred population. Symbols connected with a line depict *Tcf7*-GFP$^-$ and *Tcf7*-GFP$^+$ populations derived from the same donor mouse.

(**F**) Virus titers were determined at d8 post LCMV Arm infection in the spleen. PFU: plaque-forming units. The broken line indicates the limit of detection (L.O.D.).

(**G**) Representative flow cytometry plots depicting *Tcf7*-GFP expression among gp276 tetramer$^+$ cells following LCMV Arm challenge (d29+8). Cells derived from *Tcf7*-GFP$^-$ cells are *Tcf7*-GFP$^-$ (top). Cells derived from *Tcf7*-GFP$^+$ cells are mostly *Tcf7*-GFP$^-$ but around 5-10% of cells are *Tcf7*-GFP$^+$ (bottom).

(**H**) The number of *Tcf7*-GFP$^+$ gp276 or gp33 tetramer$^+$ cells at d0 (0) and at d8 (8) post transfer was used to calculate the fold expansion of *Tcf7*-GFP$^+$ cells in the spleen, assuming 10% take of the transferred cells. Cell number at d0 was set to 1. The expansion of *Tcf7*-GFP$^+$ cells was at least 8 fold for gp276 and 17 fold for gp33 tetramer$^+$ cells in all 5 recipients.

(**D, G, E, H**) Equivalent results were obtained for np396 (not shown). Each symbol in **E, F, H** represents data from an individual mouse. Statistics: paired t-test, n= 5. Except **F**, which is from a single experiment, all data are representative of two independent experiments. Small horizontal lines indicate the mean. Statistics: paired t-test with n= 5.

Supplemental Figure 5

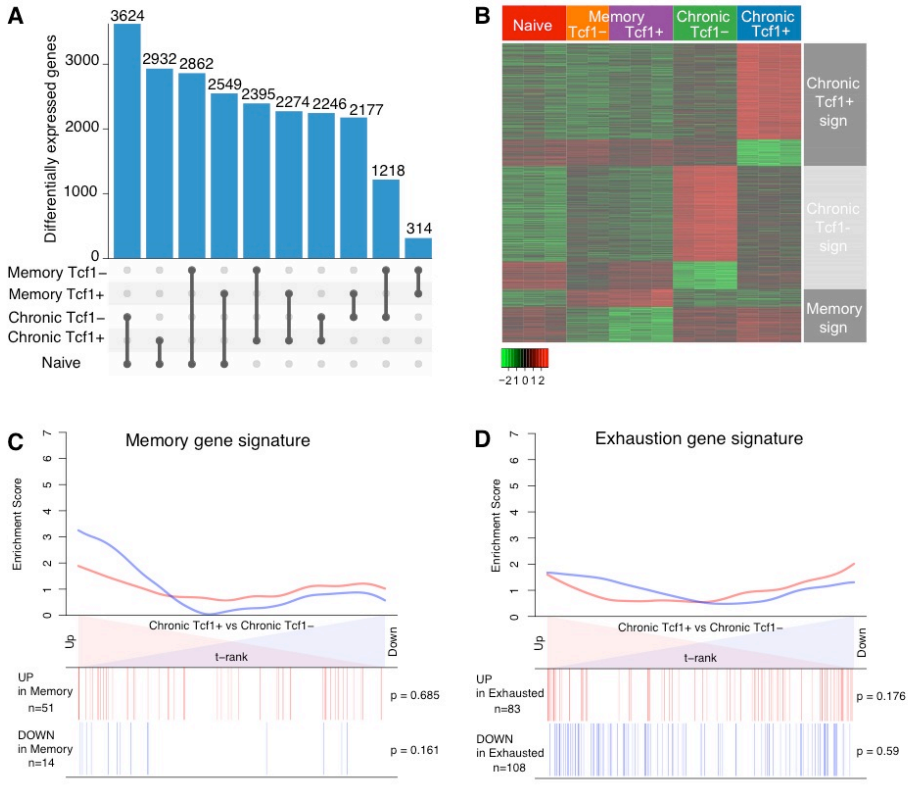

Figure S5, refers to Figure 5: Characterization of Tcf1$^+$ cells from chronic infection
(**A**) Numbers of differentially expressed genes of all pairwise comparisons. Blue bars correspond to the total number of genes found differentially expressed (FDR 5% and fold-change cutoff 2) for the comparison between the conditions indicated by the dots and edges below each bar.
(**B**) Gene signature of Chronic Tcf1$^+$ cells. Each gene signature corresponds to the overlap (intersection) of the significantly differentially expressed genes (FDR 5%; fold-change >2) when a particular cell population is compared to all other counterparts. The heatmap consists of 498 genes displaying a significant differential expression uniquely in chronic Tcf1$^+$ cells (391 up-regulated and 107 down-regulated), 502 genes unique to chronic Tcf1$^-$ cells (389 up-regulated and 113 down-regulated) and 216 genes unique to Tcf1$^+$ memory cells (72 up-regulated and 144 down-regulated). This last signature did not take into account Tcf1$^-$ memory cells.
(**C-D**) Gene set enrichment tests of memory (Acute d30) (**C**) and exhaustion (Chronic d30) gene signatures from (Doering et al. 2012) over the chronic Tcf1$^+$ versus chronic Tcf1$^-$ comparison ranked by the t-statistic. Barcode plots indicating relative enrichment scores for 51 up-regulated genes (red) and 14 down-regulated genes (blue) in the memory signature (**C**) and for 83 up-regulated genes (red) and 108 down-regulated genes (blue) in the exhaustion signature (**D**).

Supplemental Figure 6

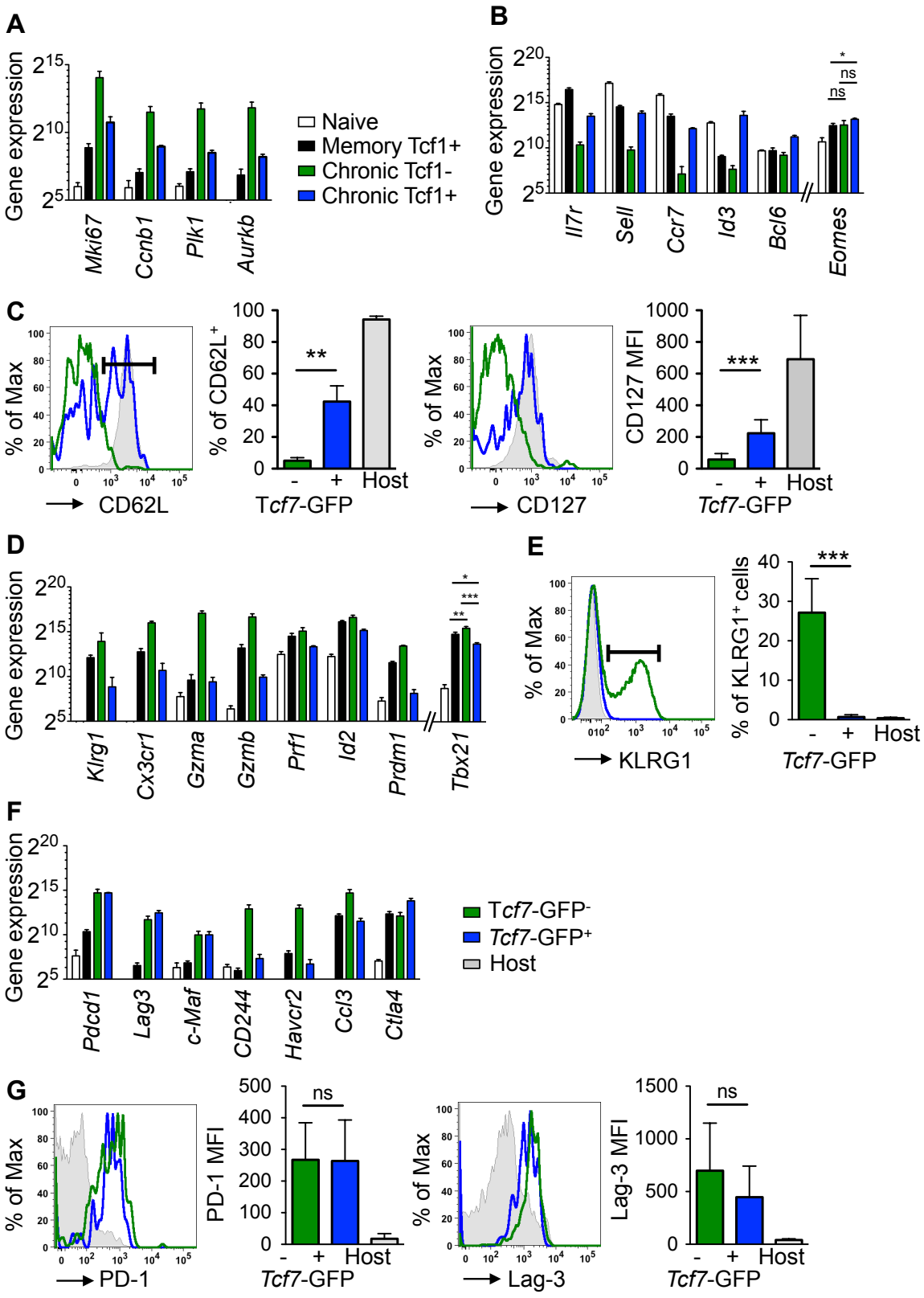

Figure S6, refers to Figure 5: Analysis of selected memory, effector and exhaustion-related features in chronic Tcf1⁺ cells

(**A**) Expression of selected cell division related genes in naive, Tcf1$^+$ memory, chronic Tcf1$^-$ and chronic Tcf1$^+$ P14 cells.
(**B, C**) Analysis of memory characteristics (**B**) Expression of selected memory related genes in naive, Tcf1$^+$ memory, chronic Tcf1$^-$ and chronic Tcf1$^+$ P14 cells. (**C**) Expression of CD62L (gp33 tetramer$^+$) and IL7Rα (CD127) (gp276 tetramer$^+$) by polyclonal *Tcf7*-GFP$^+$ (blue) and *Tcf7*-GFP$^-$ cells (green) as compared to naive (CD44$^-$) host CD8 T cells present in the spleen at d32 of c13 infection. Bar graphs depict the mean % CD62L$^+$ cells or the MFI of CD127 staining (±SD) of n=5 and n=8 determinations, respectively.
(**D, E**) Analysis of effector-related features. (**D**) Expression of selected genes involved in effector differentiation or function in P14 cells. (**E**) Expression of KLRG1 by polyclonal gp276 tetramer$^+$ *Tcf7*-GFP$^+$ and *Tcf7*-GFP$^-$ cells from the spleen of c13 infected mice. Bar graph depicts the mean % KLRG1$^+$ cells (±SD) of n=9 determinations.
(**F, G**) Analysis of exhaustion-related features. (**F**) Expression of selected genes associated with exhaustion in the indicated population of P14 cells. (**G**) Expression of PD-1 (gp33 tetramer$^+$) and Lag-3 (gp276 tetramer$^+$) by polyclonal *Tcf7*-GFP$^+$ and *Tcf7*-GFP$^-$ cells from the spleen of c13 infected mice. Bar graphs depict the mean MFIs of PD-1 or Lag-3 staining (±SD) of n=10 and n=5 determinations, respectively.
The bar graphs related to phenotypic analysis are compiled from one (CD62L, Lag-3) or two independent experiments (all others). Statistics paired t-test. The bar graphs depicting gene expression analysis show mean relative expression (±SD) derived from 3 independent samples. Note that data are shown using a log2 scale and that differences mentioned in the text are statistically significant based on one way Anova together with Bonferronis multiple comparison test. Statistics is shown for *Eomes* and *Tbx21* (T-bet) whereby ns is not significant.

Supplemental Table 4: Patient information

Patient #	Gender	Age (yr)	HCV genotype	Viral load IU/ml	HLA-A*02 Tetramer
1	F	62	1a	6079634	$NS3_{1406-1415}$
2	F	59	1a	297322	$NS3_{1073-1081}$
3	F	62	1a	680265	$NS3_{1406-1415}$; $NS5B_{2594-2602}$
4	M	53	1a	453470	$NS3_{1073-1081}$
5	M	43	3	167544	$NS3_{1073-1081}$
6	M	56	3	not determined	$NS3_{1073-1081}$
7	M	30	3	not determined	$NS3_{1073-1081}$

Supplemental Experimental Procedures

Viral infection
The LCMV 53b Armstrong (Arm) and LCMV clone 13 (c13) strains were propagated in baby hamster kidney cells and titrated on Vero African green monkey kidney cells according to an established protocol (Battegay et al., 1991). Frozen stocks were diluted in PBS; 2×10^5 plaque forming units (PFU) of LCMV-Arm were injected intraperitoneally, and 2×10^6 plaque forming units of LCMV c13 were injected intravenously. Blood samples, kidney or spleen suspensions from LCMV-infected mice were 'shock frozen'. Diluted samples were used for infection of Vero cells, and viral titers were determined by an LCMV focus-forming assay (Battegay et al., 1991).

In vivo antibody treatment
Mice were injected intraperitoneally with 200□g of rat anti-mouse PD-L1 (10F.9G2), PD-1 (RMP1-14) or rat IgG2b isotype control (LTF-2) every third day starting on d15 or d23 post infection.

Purification of mouse T cells and adoptive cell transfers
Single cell splenocyte suspensions were obtained by mashing total spleens through a 100 μm nylon cell strainer (BD Falcon). Red blood cells were lysed with a hypotonic ACK buffer. $CD8^+$ T-cells were isolated using mouse $CD8^+$ T-cell enrichment kits (Miltenyi Biotech, Bergisch-Gladbach, Germany or StemCell Technologies). One-$2x10^3$ $CD45.1^+$ or $CD45.2^+$ naïve congenic *Tcf7*$^{-/-}$ or Wt P14 T-cells were transferred into naïve $CD45.1^+$ $CD45.2^+$ C57BL/6 mice. A tenfold higher number of cells was used in Vβ5 hosts. P14 T-cells were enriched from infected mice by staining total splenocytes with anti-CD8□ (eBioscience, 53-6.7) and CD45.1 (A20) or CD45.2 (clone 104) (both prepared in house). $CD8^+$ $CD45.1^+$ or $CD8^+$ $CD45.2^+$ cells were isolated by fluorescence activated cell sorting. The purity of sorted cells was greater than 99%. Chronic infection was confirmed by staining grafted cells for PD-1 and/or Lag-3. The fold expansion of P14 T-cells in secondary hosts was determined relative to an estimated 10% "take" of transferred input cells (Blattman et al., 2002).

Surface and intracellular staining and fluorescent activated cell sorting of mouse cells.
Surface staining was performed with mAbs for 30 min and with tetramers for 90 min at 4°C in PBS supplemented with 2% FCS and 0.01% azide (FACS buffer) using the following antibodies to: CD8α (53-6.7), CD127 (SB/199), Lag-3 (eBioC9B7W), KLRG1 (2F1) (all eBioscience); Ly108 (Slamf6) (330-A), PD-1 (RMP1-30) (all Biolegend); CD62L (Mel-14) (DOF-UNIL). Tetramers (D^b/gp33-41, D^b/gp276-286 and D^b/NP396-404) were obtained from TCMetrix (Lausanne, Switzerland). Anti-CD4 (GK1.5), CD45.1 (A20), and CD45.2 (clone 104) were obtained from or custom purified by BioXCell (West Lebanon, NH, USA) and coupled to pacific blue, Alexa647, or FITC using labeling reagents from Invitrogen (Zug, Switzerland) or obtained from eBioscience.
The following antibodies were used for analyzing human HCV-specific $CD8^+$ T cells: (i) anti-CD45RA (HI100), F(ab)2 anti-rabbit IgG, anti-Eomes (WD1928), anti-CD127 (eBioRDR5) (all eBioscience); (ii) anti-CD8 (RPA-T8), anti-CD14 (M5E2), anti-CD19 (HIB19), anti-CCR7 (150503) (all BD); and (iii) anti-PD-1 (EH12.2H7, BioLegend). Viability Dye eFluor 506 (eBiosciences) was used for the exclusion of dead cells.
Stained cells were analyzed directly or washed twice and fixed in PBS supplemented with 1% formaldehyde, 2% glucose and 0.03% azide for 20 min at 4C. Then, cells were washed again and resuspended in FACS buffer.
For intracellular cytokine staining, splenocytes were re-stimulated *in vitro* with gp33-41 (gp33) peptide (5□M) for 5h in the presence of Brefeldin A (7 μg/ml) for the last 4.5h, fixed and permeabilized (using kits from BD or eBiosceince) and stained with mAbs for IFNγ□(XMG1.2), TNF (MP6-XT22) and IL-2 (JES6-5H4, all from eBioscience) or Granzyme B (GB12, Invitrogen). Transcription factors were detected using the transcription factor staining kit from eBioscience and staining with mAbs for Eomes (Dan11mag), T-bet (eBio4B10) (both from eBioscience) or Tcf1 (C63D8, Cell Signaling) followed by anti-rabbit IgG PE (eBisocience).
Flow cytometry measurements of cells were performed on an LSR-II or FACSCanto II flow cytometer (BD). All data were analyzed using FlowJo (TreeStar). For cell sorting, living cells were stained in 10% FCS RPMI media and sorted on a FACSAria (BD).

Human HCV-specific $CD8^+$ T cells.
Seven HLA-A*02-positive (HLA-A*02^+) subjects with chronic HCV infection (**Supplementary Table 4**) attending the University Hospital of Freiburg were included in the study. Written informed consent was obtained in all cases, and the study was conducted in accordance with federal guidelines, local ethics committee regulations, and the Declaration of Helsinki (1975). Approval was obtained from the ethics committee of the Albert-Ludwigs-Universität, Freiburg, Germany. Peripheral blood mononuclear cells (PBMCs) were isolated from EDTA-anticoagulated blood by density gradient centrifugation. Tetramer enrichment procedures were performed as described previously(Nitschke et al., 2015). $CD8^+$ T cell subset in healthy donors were defined based on CD45RA, CD28 and CCR7 surface

expression: Naïve: $CD45RA^+CD28^+CCR7^+$; Central memory: $CD45RA^-CD28^+CCR7^+$; Effector cells: $CD45RA^-CD28^-CCR7^-$ and $CD45RA^+$ effector memory (EMRA) cells: $CD45RA^+CD28^-CCR7^-$).

RNA-seq analysis.

Sorted GFP^+ $CD8^+$ T cells from a naive P14 *Tcf7*-GFP reporter mouse were used to obtain RNA ("naïve") or adoptively transferred into B6 ($CD45.1/2^+$) or Vβ5 ($CD45.1^+$) hosts followed by infection with LCMV Arm or c13, respectively. Data are derived from 3 replicate series (2 for $Tcf1^-$ memory) each using a distinct donor mouse. At d28 post infection splenocytes were enriched for CD8 T cells using the EasySep Mouse $CD8^+$ T Cell Isolation Kit (StemCell Technologies) and GFP^+ and GFP^- P14 cells ($CD45.2^+/1^-$) were flow sorted. Cells were lysed and stored in Trizol before extraction of total cellular RNA using the Direct-zol™ RNA MiniPrep kit (Zymo Research).

Double stranded cDNA for RNA-seq library preparation was generated using SMART-Seq v4 Ultra Low Input RNA reagents (# 634888, Clontech) according to the protocol provided with the reagents beginning with 5 ng of total RNA and using 9 cycles of PCR. 150 pg of the resulting cDNA were used for library preparation with the Illumina Nextera XT DNA Library reagents (# 15032354, Illumina) using the single cell RNA-seq library preparation protocol developed for the Fluidigm C1 (Fluidigm). Cluster generation was performed with the libraries using the Illumina TruSeq SR Cluster Kit v4 reagents and sequenced on the Illumina HiSeq 2500 using TruSeq SBS Kit v4 reagents. Sequencing data were processed using the Illumina Pipeline Software version 1.82.

Purity-filtered reads were adapters and quality trimmed with Cutadapt (v. 1.3) (Martin et al., 2011) and filtered for low complexity with seq crumbs (v. 0.1.8). Reads were aligned against *Mus musculus* (version GRCm38) genome using STAR (v. 2.4.2a) (Dobin et al., 2013). The number of read counts per gene locus was summarized with htseq-count (v. 0.6.1) (Anders et al., 2015) using *M. musculus* (Ensembl v. GRCm38.82) gene annotation. Quality of the RNA-seq data alignment was assessed using RSeQC (v. 2.3.7) (Wang et al., 2012).

Statistical analysis was performed for genes in R (R version 3.1.2). Genes with low counts were filtered out according to the rule of 1 count per million (cpm) in at least 1 sample. Library sizes were scaled using TMM normalization (EdgeR v 3.8.5) (Robinson et al., 2010) and log-transformed with limma voom function (R version 3.22.4) (Law et al., 2014). PCA analysis was performed on normalized counts. Differential expression was computed with limma (Ritchie et al., 2015) by fitting data into a linear model correcting for batch effect. All pairwise comparisons were calculated, moderated t-test was used for each contrast and the adjusted p-values were computed by the Benjamini-Hochberg (BH) method controlling for false discovery rate (FDR) independently.

Gene signatures for chronic $Tcf1^+$, chronic $Tcf1^-$ and $Tcf1^+$ memory cells were independently extracted from the pairwise comparisons by taking the intersection of the significantly differentially expressed genes (FDR 5%; absolute fold-change (fc) >2) in all comparisons including the cell population for which the signature was computed. For gene ontology and KEGG pathway enrichment analysis, we used David (Huang da et al., 2009), using only protein-coding genes as a reference list (Huang da et al., 2009).

Normalized data from published microarray experiments (Doering et al., 2012) was downloaded from GEO database (GSE41867). Differential gene expression between effector cells (Acute d8 and Chronic d8), memory cells (Acute d30) and exhausted cells (Chronic d30) versus naive cells was computed with limma. In the same way using our RNA-seq data, comparisons of $Tcf1^-$ memory, $Tcf1^+$ memory, chronic $Tcf1^-$ and chronic $Tcf1^+$ cells were compared to naive cells. PCA analysis was performed with Z-scores computed from the p-values of these comparisons.

Gene signatures for effector cells (300 up-regulated and 180 down-regulated genes), exhausted cells (83 up-regulated and 108 down-regulated genes) and memory cells (51 up-regulated and 14 down-regulated genes) were generated from the (Doering et al., 2012) data based on the comparisons described above, applying FDR 5% and 2-fold-change cut-offs. The effector signature includes genes specifically regulated in Acute d8 or Chronic d8 samples. Gene signatures consist of gene symbols matching to Ensembl v. GRCm38.82 annotation. Gene set enrichment was tested using camera (Wu and Smyth, 2012) against the ranked lists of moderated t-statistics from the comparison of Chronic $Tcf1^+$ versus Chronic $Tcf1^-$ cells.

Supplemental References

Anders, S., Pyl, P.T., and Huber, W. (2015). HTSeq--a Python framework to work with high-throughput sequencing data. Bioinformatics *31*, 166-169.

Battegay, M., Cooper, S., Althage, A., Banziger, J., Hengartner, H., and Zinkernagel, R.M. (1991). Quantification of lymphocytic choriomeningitis virus with an immunological focus assay in 24- or 96-well plates. J Virol Methods *33*, 191-198.

Blattman, J.N., Antia, R., Sourdive, D.J., Wang, X., Kaech, S.M., Murali-Krishna, K., Altman, J.D., and Ahmed, R. (2002). Estimating the precursor frequency of naive antigen-specific CD8 T cells. J Exp Med *195*, 657-664.

Dobin, A., Davis, C.A., Schlesinger, F., Drenkow, J., Zaleski, C., Jha, S., Batut, P., Chaisson, M., and Gingeras, T.R. (2013). STAR: ultrafast universal RNA-seq aligner. Bioinformatics *29*, 15-21.

Doering, T.A., Crawford, A., Angelosanto, J.M., Paley, M.A., Ziegler, C.G., and Wherry, E.J. (2012). Network analysis reveals centrally connected genes and pathways involved in CD8+ T cell exhaustion versus memory. Immunity *37*, 1130-1144.

Huang da, W., Sherman, B.T., and Lempicki, R.A. (2009). Systematic and integrative analysis of large gene lists using DAVID bioinformatics resources. Nature protocols *4*, 44-57.

Law, C.W., Chen, Y., Shi, W., and Smyth, G.K. (2014). voom: Precision weights unlock linear model analysis tools for RNA-seq read counts. Genome biology *15*, R29.

Martin, M.T., Knudsen, T.B., Reif, D.M., Houck, K.A., Judson, R.S., Kavlock, R.J., and Dix, D.J. (2011). Predictive model of rat reproductive toxicity from ToxCast high throughput screening. Biology of reproduction *85*, 327-339.

Nitschke, K., Flecken, T., Schmidt, J., Gostick, E., Marget, M., Neumann-Haefelin, C., Blum, H.E., Price, D.A., and Thimme, R. (2015). Tetramer enrichment reveals the presence of phenotypically diverse hepatitis C virus-specific CD8+ T cells in chronic infection. Journal of virology *89*, 25-34.

Ritchie, M.E., Phipson, B., Wu, D., Hu, Y., Law, C.W., Shi, W., and Smyth, G.K. (2015). limma powers differential expression analyses for RNA-sequencing and microarray studies. Nucleic acids research *43*, e47.

Robinson, M.D., McCarthy, D.J., and Smyth, G.K. (2010). edgeR: a Bioconductor package for differential expression analysis of digital gene expression data. Bioinformatics *26*, 139-140.

Wang, L., Wang, S., and Li, W. (2012). RSeQC: quality control of RNA-seq experiments. Bioinformatics *28*, 2184-2185.

Wu, D., and Smyth, G.K. (2012). Camera: a competitive gene set test accounting for inter-gene correlation. Nucleic acids research *40*, e133.